The challenging application of cosmogenic dating methods in residual glacial landforms: the case of Sierra Nevada (Spain)

David Palacios[a], Antonio Gómez-Ortiz[b], Jesús Alcalá-Reygosa[c], Nuria Andrés[a], Marc Oliva[b], Luis Miguel Tanarro[a], Ferran Salvador-Franch[b], Irene Schimmelpfennig[d], José M. Fernández-Fernández[a], Laëtitia Léanni[d], ASTER Team[d]

[a] Departament of Geography, Universidad Complutense de Madrid, Madrid, Spain
[b] Departament of Geography, Universitat de Barcelona, Barcelona, Spain
[c]Facultad de Filosofía y Letras, Universidad Nacional Autónoma de México, Ciudad de México, Mexico
[d] Aix-Marseille Université, CNRS, IRD, Coll. France, UM 34 CEREGE, Aix-en-Provence, France

Corresponding author: davidp@ucm.es (D. Palacios)

Abstract

An accurate review of the literature on surface exposure dating methods shows evidence of the difficulty in applying cosmogenic dating methods to old moraines because of the intensity of late Quaternary erosion processes. Moreover, as in some previous cases, we also found special difficulties in applying these methods to LIA moraines, caused by the intensity of current paraglacial processes. The objective of this study is to apply cosmogenic dating methods to very old and very young moraines, which in both cases have been or are being affected intensively by erosion. With this purpose, we collected samples of boulders from moraines corresponding to (i) the penultimate glaciation and (ii) the Little Ice Age (LIA), both from Sierra Nevada in the south of the Iberian Peninsula. The sampling strategy was based on a preliminary accurate analysis of the geomorphological settings of two valley sites that resulted in the collection of only four boulder samples from an old moraine and three more from a very recent moraine. Using in situ-produced cosmogenic ^{10}Be to date these boulders, the old samples yielded an age of ca. 130–135 ka for moraine stabilization. The younger samples indicate that the LIA moraine accretion probably occurred between the fourteenth and seventeenth centuries, with a subsequent stage of accumulation during the nineteenth century as suggested by historical documents. Dating a glaciation that occurred prior to the last Pleistocene glacial cycle and dating LIA glacial stages are novel in the context of Iberian glaciations and agree with other palaeoenvironmental studies in Iberian and in other European mountains. The limited number of boulders adequate for cosmic-ray exposure dating prevents statistical methods to be applied, and therefore highlights the need to improve geomorphological criteria in sample selection..

Key words: Sierra Nevada, cosmic-ray exposure dating, Beryllium 10, Little Ice Age, old glaciations.

1. Introduction

Scientific knowledge on the glacial evolution of the Iberian mountains has greatly advanced over the last decade based on the application of cosmic-ray exposure (CRE) dating on moraines, erratic boulders, and polished surfaces. This method allowed inferring spatiotemporal patterns of glaciation since the maximum extent of glaciers during the last Pleistocene glacial cycle, with a focus on the Last Glacial Maximum (LGM) (García-Ruiz et al., 2010), Oldest Dryas (Palacios et al., 2017a), and Younger Dryas (García-Ruiz et al., 2016) in the main Iberian ranges such as the Cantabrian Mountains (Rodríguez-Rodríguez et al., 2016), Pyrenees (Delmas, 2015), Central System (Domínguez-Villar et al., 2013), Iberian System (Fernández-Fernández et al., 2017), and Sierra Nevada (Palacios et al., 2016).

The existence and distribution of landforms and deposits, their delimitation and mapping, generated by glacial advances prior to the last Pleistocene glaciation are known since the first geomorphological descriptions carried out in most Iberian mountains in the late nineteenth and early twentieth centuries, such as in the Pyrenees (Penck, 1883; Nussbaum, 1949; Barrère, 1953), Cantabrian Mountains (Penck, 1897; Obermaier, 1914), Central System (Penck, 1897; Obermaier and Carandell, 1917), and Sierra Nevada (Quelle, 1908; Obermaier, 1916). However, the present knowledge on calendar of development of these landforms is scarce, and it is based on CRE dating only in very few cases. In fact, the only CRE data related to the penultimate glacial cycle were obtained with 21Ne in the NW of the Iberian Peninsula (Vidal-Romaní et al., 2015). These authors found glacial evidence (moraine boulders and polished surfaces) of a maximum advance that occurred at 155 ± 30 ka 21Ne age in the Serra de Queixa, whereas polished bedrock surfaces were dated at 231 ± 48 and 131 ± 31 ka 21Ne ages in the Serra da Geres. In addition, erratic blocks were dated at 113.9 ± 7.1 ka 10Be age in the Porma valley, Cantabrian Mountains (Rodríguez-Rodríguez et al., 2016). Another erratic boulder, with a minimum ^{10}Be age of 122.2 ± 4.9 ka, was found in Ariège valley (northern Pyrenees) (Delmas et al., 2011). This scarcity of CRE data from old moraines may be owing to the problem of moraine degradation after being affected by intensive erosion, as it has been observed even in younger moraines of other regions (Putkonen and Swanson, 2003; Briner et al., 2005; Putkonen et al., 2008; Balco, 2011; Heyman et al., 2011).

The rest of the dates corresponding to glacial landforms formed during the penultimate glaciation in the Iberian Peninsula were carried out by other dating methods. Villa et al. (2013) were able to date with U/Th the limestone of cemented calcareous breccia in Duje valley, Picos de Europa, also in the Cantabrian Mountains. This breccia deposit lies on glacially abraded surfaces and is covered by moraines dated between 394 ± 50 and 276 ± 23 ka/394 ± 50 ka U/Th age. In the southern slope of the Central Pyrenees, optically stimulated luminescence (OSL) dating was applied to sandy layers in fluvioglacial terraces in two nearby valleys that show the following ages: 151 ± 11 ka in the Gállego valley (Lewis et al., 2009) and 263 ± 21 and 171 ± 22 ka in the Aragón valley (García-Ruiz et al., 2013).

In other Mediterranean mountains, landforms originated from glaciations prior to the Late Pleistocene Glaciation (LPG) have been dated by U/Th, 230Th, and OSL methods in the Balkan region (Hughes et al., 2006a, Hughes et al., 2006b, Hughes et al., 2007), Dinaric Alps (Hughes et al., 2011), and Apennines (Kotarba et al., 2001), but not through CRE dating. In comparison to the large data set of CRE ages existing for reconstructing the LPG in the Alps, only a few erratic boulders are related to the penultimate glacial cycle dated by this method (Graf et al., 2015), as it is also the case of the Himalayas (Schaefer et al., 2008). On the contrary, the application of 230Th dates on the stalagmite record in the Alps allowed determining with high resolution the last maximum ice advance of the penultimate glacial cycle at 133.1 ± 0.7 and 131.9 ± 0.6 ka. These dates coincide with Heinrich stadial 11 and the onset of the penultimate deglaciation or Termination II (TII), which started at 131.8 ± 0.6 ka (Häuselmann et al., 2015) and reached its maximum intensity at 130.9 ± 0.9 ka (Moseley et al., 2015).

However, CRE methods have never been applied to date the Little Ice Age (LIA) in the Iberian Peninsula, although this cold event has been extensively documented in this region (González-Trueba et al., 2008; Oliva et al., 2018a). The CRE dating showed that the LIA was the most extensive Holocene glacial advance in most Iberian mountains (Palacios et al., 2017b), with the exception of some cirques in the Central Pyrenees (García-Ruiz et al., 2014). In fact, after pioneer studies in New Zealand (Schaefer et al., 2009) and the Andes (Licciardi et al., 2009), the use of CRE dating methods to date landforms of Neoglacial and LIA age has just been recently applied in the Alps (Schimmelpfennig et al., 2012, Schimmelpfennig et al.,

2014; Le Roy et al., 2017), Arctic (Young et al., 2015; Jomelli et al., 2016), and Central Asia mountains (Li et al., 2016; Dong et al., 2017).

Radiocarbon dating on glacial, fluvioglacial, and lacustrine sediments (as well as speleothems, tree rings, and historical documents) established the onset of the LIA in the Iberian Peninsula at 1300 common era (CE), with the coldest conditions of ca. 2 °C below present-day values at 1620–1715 CE and the last cold episodes at 1760–1800 and 1815–1835 CE (Oliva et al., 2018a). In Sierra Nevada there were also small glaciers during the LIA that have been reconstructed based on radiocarbon dating of lake sediments (Oliva and Gómez-Ortiz, 2012) and through historical documents (Gómez-Ortiz et al., 2009, Gómez-Ortiz et al., 2018).

The objective of this work is to apply CRE methods to glacial landforms originated during advances prior to LPG and to very young moraines as well as to review and discuss those found in this research in comparison to other similar studies. Sierra Nevada constitutes a unique environment to examine the use of CRE dating as a potential tool to reconstruct the chronology of old and young glaciations, from the well-constrained glacial chronological record of the LPG and the existence of glacial landforms originated before and after this glaciation in these mountains.

2. Study area

Sierra Nevada is located in the SE of the Iberian Peninsula and runs SW-NE parallel to the Mediterranean Sea (Fig. 1). This massif includes the highest peaks of the Iberian Peninsula: Mulhacén (3478 m asl; 37°03′12″N, 3°18′41″W) and Veleta (3398 m; 37°03′02″N, 3°20′54″W). The area is composed of Paleozoic metamorphic rocks, mainly micaschists, profoundly tectonized during the Alpine orogeny, with the presence of intensive foliation and joints that makes them susceptible to intense weathering (Messerli, 1965; Sanz de Galdeano and López-Garrido, 1999). Climate conditions in Sierra Nevada are characteristic of a semiarid mid-latitude mountain environment, with a mean annual air temperature (MAAT) at 2500 m of 4.4 °C and a total precipitation of 710 mm, 40% of which falls as snow (Oliva et al., 2016a). The MAAT at the top of the Veleta peak between 2002 and 2013 was 0.08 °C, with a slight increase of 0.12 °C during this period (Oliva et al., 2016a).

The Quaternary landscape evolution of Sierra Nevada has been largely studied over the last decades (Fig. 1, Table 1). From the first basic geomorphological observations of the late nineteenth and early twentieth centuries to the recent multidating approaches, our understanding of the glacial processes shaping the landscape of the highest lands has significantly improved (i.e., Gómez-Ortiz et al., 2015).

During the 1960s and 1970s several authors suggested that the existence of older glaciations occurred prior to the LPG, formerly known as the Riss glaciation in Alpine terminology. Their observations focused on the existence of highly eroded moraine remnants and fluvioglacial deposits at very low altitudes, mainly in the southern slope of the massif (Hempel, 1960; Messerli, 1965; Lhenaff, 1977; Sánchez-Gómez, 1990). However, this hypothesis has not been validated until now though direct dating methods.

By contrast, the LPG has been recently well-constrained with CRE techniques. Gómez-Ortiz et al. (2012) and Palacios et al. (2016) reported that two major glacial advances occurred at ca. 30–32 and 19–20 ka. The second stage of glacial advance occurred in phase to the global Last Glacial Maximum and reached almost the same extent than during the previous glacial stage. Subsequently, temperature increase recorded worldwide (Clark et al., 2009) favored a massive deglaciation of the massif, although two stages of glacial expansion occurred during the transition toward the Holocene, namely during the Oldest Dryas and Younger Dryas. During these phases, glaciers expanded significantly and flowed downvalleys several kilometers, in southern and northern slopes (Gómez-Ortiz et al., 2012; Palacios et al., 2016).

The Holocene was characterized by warmer temperatures that promoted the gradual melting of these glaciers during the early Holocene (Palacios et al., 2016). The formerly glaciated environments were then subjected to paraglacial processes, which favored the development of rock glaciers associated to permafrost conditions (Oliva et al., 2016b, Oliva et al., 2018b). These permafrost-related landforms finally stabilized at 6–7 ka during the Holocene Climate Optimum, when warmer conditions must have conditioned permafrost thawing (Palacios et al., 2016).

Climate variability intensified in the Northern Hemisphere during the late Holocene (Mayewski et al., 2004). In Sierra Nevada, this was reflected in alternating cold and warm

168 phases (Oliva et al., 2014). During the coldest stages, some glacier spots developed in the
169 highest northern cirques, such as in the Mulhacén cirque, where lake sediments from La
170 Mosca Lake revealed evidence of the existence of a glacier within the cirque at ca. 2.8–2.7
171 and 1.4–1.2 ka cal BP and during the LIA between 1440 and 1710 CE (Oliva and Gómez-
172 Ortiz, 2012). For the last cold stage, historical documents also showed evidence of the
173 prevailing colder conditions in Sierra Nevada, with descriptions sketches and pictures of
174 glaciers and permanent snow fields at the foot of the highest peaks of the westernmost
175 mountains of Sierra Nevada between the late seventeenth and the early twentieth centuries.
176 The last glacier was located in the Veleta cirque and constituted the southernmost glacier in
177 Europe during the LIA, although it finally melted away during the mid-twentieth century
178 (Gómez-Ortiz et al., 2001, Gómez-Ortiz et al., 2009, Gómez-Ortiz et al., 2018; Oliva and
179 Gómez-Ortiz, 2012; Oliva et al., 2018a). However, no CRE dating is yet available from the
180 different LIA glacial stages in Sierra Nevada.

181

182

183 **3. Methods**

184 *3.1 Sampling strategy*

185 With the aim of dating glacial landforms formed potentially before the LPG, this research
186 focuses on the Naute valley, a steep mountain ravine located on the southern slope of the
187 Mulhacén peak (Fig. 1, Fig. 2, Fig. 3, Fig. 4). The valley results from the confluence of two
188 glacial headwaters — Río Seco and Mulhacén valleys — converging at 2300 m of altitude. In
189 previous studies these two high mountain valleys were selected to reconstruct glacial stages of
190 the LPG using CRE methods (Gómez-Ortiz et al., 2012; Palacios et al., 2016), but landforms
191 distributed in the lower Naute valley affected by intense erosion processes were not
192 examined. In Río Seco and Mulhacén valleys landforms from the LPG have been already
193 dated using the in situ cosmogenic nuclide 36Cl, such as the front of a fossil rock glacier (9.0
194 ± 0.8 ka) resting on polished rock surfaces (11.9 ± 1.1 ka) in the Río Seco cirque, as well as of
195 a fossil rock glacier (6.3 ± 0.5 and 13.1 ± 1.3 ka) resting on a polished rock surface (11.2 ±
196 1.1 and 12.7 ± 1.2 ka) at the head of the Mulhacén valley (Palacios et al., 2016). Just before
197 their confluence, both valleys include a sequence of moraine ridges, where five blocks were
198 dated using 36Cl (29.9 ± 2.6, 16.9 ± 1.8, 14.9 ± 1.5, 13.7 ± 1.3, and 11.7 ± 1.6 ka; Palacios et
199 al., 2016). These authors interpreted these ridges as a polygenic moraine formed by

successive advances generated from just before the LGM to the Oldest Dryas. In the Naute valley, immediately below the confluence of these two tributaries, a lateral moraine is preserved in the left sector of the valley at elevations between 2150 and 2300 m. This moraine is placed below one of the ridges where a boulder was dated at 29.9 ± 2.6 ka (Palacios et al., 2016), and therefore must be older in age, possibly from a previous glaciation. For this reason, this lower moraine was considered as one of the objectives of the work in order to apply the CRE dating method.

To date glacial oscillations during the LIA by CRE dating methods, we focused our research on the Veleta cirque, located under the northern wall of Veleta peak (Fig. 1, Fig. 5, Fig. 6). Historical documents provided abundant evidence of a glacier existing at the floor of this cirque during the LIA until the first half of the twentieth century (Gómez-Ortiz et al., 2001, Gómez-Ortiz et al., 2009, Gómez-Ortiz et al., 2018). The cirque is closed by a large frontal moraine whose age is unknown, although because of its large size it has been considered to have formed during the Last Termination or during Holocene advances (Oliva et al., 2014, Oliva et al., 2018a).

.

3.2 Sampling and analytical procedures

even samples were collected from moraine boulders using a hammer and a chisel: four located in Naute valley (NAUT-1, -2, -3, -4) between 2164 and 2263 m, and three in the Veleta cirque (SN-11-1, -2, -3) between 3061 and 3095 m (Table 1). All samples were taken from the flat-topped surfaces of boulders >1 m high, located on the crests of the moraines. Field data and sample characteristics of the seven samples are listed in Table 2.

Physical and chemical sample preparation and beryllium measurements were carried out at the Centre Européen de Recherche et d'Enseignement des Géosciences de l'Environnement (CEREGE, France). Lichen, moss and other organic fragments were removed from the samples with a brush. Samples were crushed with a roller grinder and sieved to retrieve the grain size fraction 0.25–1 mm. All samples are quartz-bearing micaschists, and therefore we selected in situ-produced cosmogenic ^{10}Be dating to determine the ages of the moraines. To isolate the quartz from the bulk rock, the samples went repeatedly through a magnetic separator (Frantz LB-1) until all magnetic minerals were discarded. Subsequently, the nonmagnetic fraction experienced successive chemical attacks with a mixture of concentrated

hydrochloric (HCl) and hexafluorosilic (H2SiF6) acids to dissolve the remaining nonquartz minerals. The residual impurities were dissolved when the sample grains were decontaminated from meteoric ^{10}Be by three successive partial dissolutions with concentrated hydrofluoric acid (HF).

The subsequent beryllium extraction protocol is adapted from Brown et al. (1991) and Merchel and Herpers (1999) chemical procedures. The samples yielded between 18 and 32 g of purified quartz (Table 3). About 100 µl of a 9Be carrier solution with a 9Be concentration of 3025 µg/g prepared in-house from a phenakite crystal was added to the quartz before it was dissolved in HF. A chemistry blank was prepared along with the seven samples. Following evaporation of the resulting solution, the samples were recovered in a hydrochloric acid solution and beryllium was precipitated to Be(OH)2 with ammonia before and after elution through an anionic exchange column (Dowex 1X8) to remove iron. Following the methods described by Merchel and Herpers (1999), a cationic exchange column (Dowex 50WX8) was used to remove boron and to separate the Be from other elements. Beryllium was precipitated with ammonia to Be(OH)2 and the resulting precipitate was oxidized to BeO at 700 °C. Then, this final BeO was mixed with niobium powder and loaded on cathodes for analysis of the ^{10}Be/^{9}Be ratios at the French national Accelerator Mass Spectrometry (AMS) facility ASTER (CEREGE) (Arnold et al., 2010). The measurements were calibrated against in-house standard STD-11 using an assigned ^{10}Be/^{9}Be ratio of 1.191 (±0.013) × 10−11 (Braucher et al., 2015). Sample ^{10}Be/^{9}Be ratios were corrected for the chemical blank background by subtracting the measured chemistry blank ^{10}Be/^{9}Be ratio (Table 3). Analytical 1σ uncertainties include uncertainties in AMS counting statistics, the uncertainty in the standard ^{10}Be/^{9}Be ratio, an external AMS error of 0.5% (Arnold et al., 2010), and the uncertainty in the chemical blank measurement. A ^{10}Be half-life of 1.387 (±0.01) × 106 years was used (Chmeleff et al., 2010; Korschinek et al., 2010).

3.3 Age calculation (^{10}Be age computation)

We calculated the ^{10}Be CRE ages with the online CREP exposure age calculator (Martin et al., 2017; http://crep.crpg.cnrs-nancy.fr), using the LSD scaling model (Lifton et al., 2014) that is similar to other previous empirical models (Borchers et al., 2016). Age calculations have also considered the ERA40 atmospheric model (Uppala et al., 2005) and LSD

Framework geomagnetic database (Lifton et al., 2014). As it is not regional production rate available, we used the worldwide mean ^{10}Be spallation production rate of 3.99 ± 0.22 atoms g−1 y−1, as calibrated in the ICE-D production rate database linked to CREP. For all samples, a rock density of 2.7 g cm−3 was considered, and the topographic shielding factor of each sample was calculated (Table 2).

In the moraine of the Veleta cirque, from where samples SN-11-1, SN-11-2, and SN-11-3 were extracted, snow cover remains for a large part of the year (Gómez-Ortiz et al., 2009); and there is information on the properties and persistence of the snow cover for the last decades (Herrero and Polo, 2016), which allows considering snow shielding effect for these samples. The correction for snow cover has been calculated applying the equation by Gosse and Phillips (2001), including local parameters (Herrero and Polo, 2016), and considering a snow thickness on moraine boulders ranging from 30 to 130 cm during 8 months per year. We used an average value of snow density of 0.3 g cm−3, considering that the attenuation length for fast neutrons in snow is 109 g cm−2 (Zweck et al., 2013; Delunel et al., 2014). Taking into account these characteristics, we applied a snow shielding factor of 0.865 to the affected samples. We have not applied a snow shielding factor to the old samples of Naute moraine, as the coverage of snow in this area is much shorter and data are not available for a period encompassing several tens of thousands of years.

Table 3 also includes the ages determined with version 3 of the online exposure age calculator formerly known as the CRONUS-Earth online exposure age calculator (Balco et al., 2008; Balco, 2018). These ages have been calculated using the default calibration data set based on the ICE-D calibration database and the time-dependent LSDn scaling method (Lifton et al., 2014). The average difference between the ages calculated with the CREP exposure age calculator and those calculated with the CRONUS-Earth (v.3) is 2.4% for NAUT samples and 6.9% for SN-11 samples.

The ages of the SN-11 samples calculated with the snow shielding factor turn out to be between 8.8 and 16.9% higher in the online CREP exposure age calculator (Martin et al., 2017) and between 7.9 and 16.9% higher in the online exposure age calculator formerly known as the CRONUS-Earth online exposure age calculator v. 3 (Balco et al., 2008; Balco,

2018). The CREP exposure calculator ages and the analytical uncertainties are used in the text and in the figures of this manuscript and, only in the case of the Veleta cirque, with the application of the snow shielding factor (Table 3).

4. Results

4.1 Geomorphological analysis of the Naute moraine and CRE dating results

To select the most suitable boulders for CRE dating, an exhaustive survey was carried out of the Naute moraine system, formed potentially during a glacial advance before the LPG. The results of this survey are expressed in a detailed geomorphological map (Fig. 2). The moraine is located on the left bank of the Naute river (west) and the Peñón Grande (east) between 2150 and 2300 m. It has been intensely reshaped by postglacial environmental dynamics (i) fluvial processes driven by steep streams have deeply eroded the moraine ridge, and (ii) gullying processes have washed away a large part of its abundant fine sediments. As a result, a large number of boulders — highly weathered and fragmented caused by their abundant foliation planes and joints — are found on the surface of the moraine (Fig. 3).

To sample the boulders that best represent the original surface of the moraine, we focused on blocks that (i) present aligned upper edges indicating the maximum possible height of the original moraine crest, and (ii) are inserted into the moraine, which ensures that they have not been mobilized since the moraine stabilization. Using these criteria, only four boulders were found with these characteristics (NAUT-1, -2, -3, and -4) (Fig. 4). The rest of the boulders showed traces of having been affected by erosion and exhumed.

Samples from two boulders showed a similar age: NAUT-1 yielded 134.8 ± 6.2 ka and NAUT-4 129.2 ± 5.3 ka. The other two boulders showed different and substantially younger ages: NAUT-2 obtained 53.7 ± 2.9 ka and NAUT-4 43.8 ± 2.3 ka (Fig. 2, Fig. 3; Table 3).

4.2 Geomorphological analysis of the Veleta cirque moraine and CRE dating results

The Veleta cirque moraine is composed of a large proportion of fine sediments with a few large blocks on the surface, possibly deposited by different glacial advances. Within the area enclosed by this moraine, there are large rock avalanche deposits fallen from the Veleta

northern wall and a small rock-glacier where buried glacial ice is still preserved under the debris cover, though it presents evidence of accelerated degradation. On the other hand, the fine sediments of the moraine, resulting from heavily weathered micaschists, are being washed away by runoff activity. This process is particularly intense in late spring and early summer with snowmelt runoff and in autumn with torrential rain events. The outer slope of the moraine is being reshaped by frequent debris flows, which also facilitate the outcropping and exhumation of large blocks buried in the moraine. In addition, some metric-size boulders are present fallen from the Veleta north wall and deposited on the surface of the moraine, normally during the winter season when snow completely fills the floor of the cirque. These rocks slide on the snow and ice surface and stabilize on the moraine ridge. On the inner slope of the moraine, accumulations are found of superimposed till blocks of different sizes. In contrast to the main moraine, these till deposits include a smaller proportion of fine particles but conserve a recent glacial imprint as revealed by the presence of flutes. This deposit exceeds the limits of the main moraine on the eastern side of the cirque, where the moraine height is lower (Fig. 5, Fig. 6). Evidence from historical sources confirms that the distribution of this recent till deposit coincides with the surface covered by the glacier during the nineteenth century (Fig. 7; Bide, 1893; Gómez-Ortiz et al., 2018).

Before selecting boulders for CRE dating, a very detailed geomorphological survey of the large polygenic moraine system enclosing the Veleta cirque was conducted. A detailed geomorphological map shows the main landforms observed in the cirque (Fig. 5). Schematic transects show the sectors of the moraine affected by current or recent post-glacial processes and derived landforms (Fig. 6). Considering these geomorphological characteristics, we avoided collecting samples from blocks corresponding to very recently deglaciated surfaces because (i) we already know that this area was occupied by the glacier during the nineteenth century and (ii) they can result from the frequent rockfalls from the headwall. As a result, only three CRE datable boulders were found anchored in the moraine and protruding sufficiently not to have been covered by other sediments since their deposition (SN11-1, -2, and -3) (Fig. 7). Thus, they cannot have fallen from the headwall or have been covered by the glacier in a subsequent readvance.

Sample SN-11-1, collected on the top of the moraine, very close to twentieth century till deposits, obtained an age of 340 ± 120 years, corresponding to the year 1675 ± 120 CE. Sample SN-11-2, collected on the crest of the lobate ridge of the moraine, yielded an age of

720 ± 270 years (1295 ± 270 CE). Finally, sample SN-11-3, collected on the top of the lateral moraine ridge in the western part of the cirque, obtained an age of 400 ± 110 years (1615 ± 110 CE) (Fig. 5, Fig. 6; Table 3).

5. Discussion

5.1 The existence of a glaciation prior to the last Pleistocene cycle in Sierra Nevada

The results of ^{10}Be CRE dating yielded ages of ca. 130–135 ka for the two samples collected from boulders in the moraine downslope of the maximum ice advance in Sierra Nevada (Gómez-Ortiz et al., 2012). These ages suggest that the moraine may have been formed during the last maximum advance of the penultimate glaciation. The other two boulders of the same moraine yield much younger ages, around 45–50 ka (Table 3), and thus can be considered outliers. On the other hand, none of the studies in Sierra Nevada reported boulder samples affected by nuclide inheritance (Gómez-Ortiz et al., 2012, Gómez-Ortiz et al., 2015; Palacios et al., 2016), and therefore this problem can be rejected in the older samples (Fig. 8).

In Sierra Nevada, no polished and striated bedrock surfaces were found in this study between the moraine ridges dated ca. 130–135 ka and those dated in previous studies between ca. 30 and 15 ka (Palacios et al., 2016), i.e., rock surfaces that may have been ice-covered prior to the LPG. All the polished bedrock surfaces dated in Sierra Nevada — in many cases with abundant and well-preserved fresh striations — correspond to the deglaciation process during Termination I (Gómez-Ortiz et al., 2012; Palacios et al., 2016). The fact that moraines from a previous glaciation are found in close proximity to those of the last glacial cycle without intermediate polished surfaces led us to apply CRE dating only on boulder surfaces in the old moraines. Recent research in mountain areas, such as in the Alps (e.g., Chenet et al., 2016), the Andes (e.g., Martini et al., 2017), Central Asia (e.g., Batbaatar et al., 2018), and the Iberian Peninsula (Rodríguez-Rodríguez et al., 2016, Rodríguez-Rodríguez et al., 2017), suggest using a minimum of five boulders from the same moraine to ensure obtaining the formation age of the landform. Thus, where most of the results show dispersed data, the ages are rejected, whereas an average value is obtained with the rest, interpreted as indicative of the development age of the moraine. In this study we attempted to apply this five-boulder criterion, but this proved impossible because of the deterioration of the moraine since the penultimate glaciation, as the landform has been intensely eroded and few potentially datable

393 boulders are available. The headwaters of several torrents have eroded the ridge summit,
394 leaving the moraine covered with loose blocks. When trying to reconstruct the original
395 surface of the moraine, we found only four embedded boulders (Fig. 4).

396

397 The CRE ages of ca. 130–135 ka obtained in Sierra Nevada coincide with the last cold period
398 of the penultimate glaciation in the Alps as suggested by 230Th dating on speleothems that
399 obtained 131.8 ± 0.6 ka (Häuselmann et al., 2015; Moseley et al., 2015). This stage occurred
400 during Heinrich stadial 11 (Oppo et al., 2006), parallel to the end of the last cold phase in the
401 Alboran sea surface temperatures (near Sierra Nevada, in SE Iberia) before the beginning of
402 TII (Martrat et al., 2014; Jiménez-Amat and Zahn, 2015). By that time, the onset of warmer
403 temperatures favored the end of the last cold period of the penultimate glaciation in Greenland
404 (Grant et al., 2012) as well as the initial melting of large ice sheets at high latitudes in the
405 Northern Hemisphere (Govin et al., 2015), leading to sea level rise (Rohling et al., 2017).

406

407 The formation and stabilization of the Naute moraine may therefore be contemporary with
408 what is called the Penultimate Glacial Maximum (PGM), a parallel concept to the LGM for
409 the last glaciation, centered on 140 ka (Rohling et al., 2017). The deposition age of the Naute
410 moraine is similar to the stabilization age of the maximum glacial advance moraine in the
411 Sierra de Queixa dated 155 ± 30 ka 21Ne (Vidal-Romaní et al., 2015). The erratic boulder
412 dated 113.9 ± 7.1 ka ^{10}Be in the Porma Valley, Cantabrian Mountains, could also be related to
413 the deglaciation process following the PGM (Rodríguez-Rodríguez et al., 2016). The same is
414 true for the erratic boulder in the Ariège valley (northern Pyrenees), with a minimum ^{10}Be age
415 of 122.2 ± 4.9 ka (Delmas et al., 2011), slightly after the formation of the Naute moraine from
416 the penultimate glaciation. In addition, fluvioglacial terraces deposited simultaneously on the
417 outermost moraine ridges in the Gállego and Aragón valleys, Central Pyrenees, were dated
418 151 ± 11 ka and 171 ± 22 ka OSL ages by other authors (Lewis et al., 2009; García-Ruiz et
419 al., 2013), and therefore may represent the same glacial stage that led to the formation of the
420 Naute moraine. However, despite some evidence suggesting glacial activity between ca. 170
421 and 130 ka in the Iberian Peninsula, the small number of reliably dated terrestial records
422 makes it difficult to infer spatiotemporal glaciation patterns occurring before the LPG. This is
423 a common issue in other Mediterranean mountains where glacial advances concurrent with
424 the development of the Naute moraine have only been dated through the application of U

425 series to secondary carbonates in cemented moraines in mountains in Greece (Hughes et al.,
426 2006a, Hughes et al., 2006b, Hughes et al., 2007), Dinaric Alps (Hughes et al., 2007) and the
427 Gran Sasso Massif, Central Italy (Kotarba et al., 2001).

428

429 A case study similar to the Naute moraine was undertaken in the Jura mountains, where
430 several erratic boulders were found scattered beyond the Alpine glaciers LGM extent. In this
431 case the oldest ages were very similar to those of the Naute moraine (129.7 ± 4.7 ka, 143.2 ±
432 8.2, and 144.0 ± 5.3 ka ^{10}Be ages), although just as in Sierra Nevada, other boulders in the
433 same deposit yielded younger ages (Graf et al., 2015). After their experience applying CRE
434 dating to several moraine boulders in the Himalayas, Schaefer et al. (2008) highlighted the
435 role of erosion processes in the exhumation of blocks in old moraines. As a result, these
436 authors claim that the oldest, not the average age of the moraine boulders reflects the best
437 minimum age estimation for the moraine deposition, in agreement with previous authors
438 (Hallet and Putkonen, 1994). Briner et al. (2005) proposed the same criterion after analyzing a
439 large number of moraine boulders, presumably from the penultimate glaciation in Alaska, and
440 found many problems of boulder exhumations. These authors also defend an oldest-age
441 method to provide the closest approximation to the moraine stabilization age. Similarly, and
442 from previous experience, Balco (2011) defined the most appropriate strategies when
443 applying CRE methods to degraded moraines, which have been considered in this study.

444

445 From our results we conclude that the difficulty of finding suitable boulders to apply CRE
446 methods in moraines from old glaciations should not discourage their use. Dating an adequate
447 number of samples is very difficult for moraines prior to the LPG, where erosive activity over
448 time may have exhumed most of the boulders. In the case of Sierra Nevada, the profoundly
449 tectonized micaschists have been intensely affected by erosion, which makes it more difficult
450 to find suitable boulders for dating (Gómez-Ortiz et al., 2015). Nevertheless, Sierra Nevada is
451 an arid mountain, where ice margin deposits preserved on gentle slopes make it possible to
452 obtain a well-dated glacial sequence using the CRE method (Pallàs et al., 2010) (Fig. 9).

453

454 *5.2 Chronology of the formation of LIA moraines in Sierra Nevada*

455 It was also difficult to find suitable blocks for CRE dating in young moraines in Sierra
456 Nevada, as they are found in very dynamic geomorphological environments on steep slopes of

200 m high (up to 300 m from the peaks to the cirque floors) with thick and long-lasting snow cover. On the one hand, these factors accelerate erosion processes in the moraine, often reducing its size, vertical development, and the slope gradient; on the other hand, they favor new sediment deposits on the moraine surface. These difficulties are also observed in most Mediterranean mountains, where LIA glaciers did not exceed the limits of the cirques and developed at the foot of vertical walls (Hughes, 2014, Hughes, 2018). Previous studies adverted to the polygenic character of the Veleta cirque moraine, related to the effects of an Early Holocene glacial advance that pushed downslope, accumulating rockfall deposits from the end of TI (Gómez-Ortiz et al., 2012; Palacios et al., 2016). According to these authors, this moraine system functioned as a barrier to subsequent advances, which accumulated sediments on the inner slope, generating a single, large, polygenic moraine.

Using the criteria defined in Methods above, we obtained three coherent results to infer the age of the moraine, although dates were obtained for only three boulders. The high uncertainty levels in our results prevent us from relating the age of each sample to LIA periods (Oliva et al., 2018a). These ages could be related to advances from 1300 to 1610/1680 CE, contemporary with the LIA maximum glacial advance in the Alps (Holzhauser et al., 2005) and the lowest temperatures in the Iberian Peninsula during the Maunder Minimum (Oliva et al., 2018a).

The inner slope of the moraine therefore developed during the LIA, although the large moraine system may also include boulders from other Neoglacial glacial stages, such as those detected in the Mulhacén cirque where lake sediments show evidence of a glacier within the cirque ca. 2.8–2.7 and 1.4–1.2 ka cal BP and LIA (Oliva and Gómez-Ortiz, 2012).

New results obtained in Mount Olympus (Greece) found similar results using 36Cl dating method, with one sample of 0.64 ± 0.08 ka (Styllas et al., 2018). However, most studies focusing on the use of CRE dating methods for dating LIA glacial advances have been carried out in the Alps. In the Western Alps, LIA moraines are very close to Neoglacial (Late Holocene) moraines and may even overlap them (Schimmelpfennig et al., 2012, Schimmelpfennig et al., 2014); as in the Veleta cirque, LIA glacial advances have left a single polygenic ridge with dated boulders showing a wide range of dates: 1430 ± 32, 1534 ± 28,

and 1829 ± 11 CE ^{10}Be (ages not considering snow shielding) (Schimmelpfennig et al., 2012). These dates could correspond to the three most important glacial advances in the Alps during the LIA: 1300–1380, 1600–1670, and 1800–1860 CE (Holzhauser et al., 2005), similar to those detected in the Pyrenees (Oliva et al., 2018a). Recent studies in the central Alps showed a similar pattern when dating LIA moraine boulders — also very close to or overlapping Neoglacial moraines — forming single polygenic crests (Schimmelpfennig et al., 2014). These authors dated 14 boulders in a single LIA moraine ridge using ^{10}Be, assuming negligible inheritance for the boulders, and reported dates ranging from 1430 to 1870 CE (Schimmelpfennig et al., 2014). Le Roy et al. (2017) dated Neoglacial moraines near several present-day glacier fronts in the French Alps and obtained ^{10}Be ages that are all consistent with the late Holocene period (~4–1 ka), but do not follow the logical chronostratigraphic moraine sequence. These authors highlighted the problems related to surface exhumation and erosion of many moraine ridges.

Some attempts to date the moraines of the LIA have also been made in other high mountain ranges such as the Cordillera Vilcabamba, central Andes where Licciardi et al. (2009) applied ^{10}Be CRE dating for the first time. Samples collected from a single massive ridge showed average dates ranging from 1740 ± 30 to 1810 ± 20 CE, though samples of old dates were rejected as being outliers. They suggest that the moraines found in several valleys of this massif may be the result of the successive accumulation of multiple late Holocene glacial expansions.

Schaefer et al. (2009) also applied ^{10}Be dating in the Mueller valley in the Southern Alps, New Zealand, to date many LIA moraine boulders. The geomorphological setting is similar to that described in the European Alps, with a single LIA moraine system overlapping with various late Holocene moraine ridges. Boulders taken from different sites in the LIA moraine reported dates of 1350 ± 60, 1600 ± 50, 1780 ± 40, and 1820 ± 20 CE ^{10}Be, which coincide with cold periods inferred from tree-ring data. Li et al. (2016) applied ^{10}Be dating in LIA moraines in Tian Shan mountains, central Asia; interestingly, they found that boulders in moraines from glaciers smaller than 1.0 km2 show very old ages because of nuclide inheritance. The same problems were found in the small Veleta cirque, where the wall is very close to the moraine, but we discarded this possibility following the results obtained in this

present study and those from other previous work in Sierra Nevada, because of the intense, continuous rock fall activity on its wall. For larger glaciers, Li et al. (2016) found evidence of a major advance ca. 1600 ± 100 CE ^{10}Be and also a remarkable early LIA glacial expansion at ca. 1480 ± 55 CE ^{10}Be. Dong et al. (2017) dated two different LIA ridges in Tibetan mountains with ^{10}Be, collecting four samples from each ridge. Their results provide a range of 1480 ± 139 to 1975 ± 31 CE ^{10}Be dates for the entire moraine system, very similar to the Veleta cirque results. Young et al. (2015) dated several stable moraine ridges close to the current alpine glacier snouts in Baffin Island and western Greenland and found a logical geomorphological order from 1040 ± 40 to 1700 ± 40 CE ^{10}Be ages with a retreat from 1750 CE and proposed a recent glacial maximum during the Medieval Climate Anomaly, when glaciers in Europe receded. Jomelli et al. (2016) applied in situ cosmogenic 36Cl to date three moraines in Lyngmarksbræen glacier (west Greenland), which were deposited during the last millennium in a relatively flat area not constrained by topography, the opposite that happens in Alpine environments. These authors obtained advances with average ages of 1200 ± 130, 1450 ± 90, and 1720 ± 60 CE for the most external and internal ridges. The most recent advances coincide with glacial expansion in European high mountains, but the older moraine may have developed during the Medieval Climate Anomaly (Jomelli et al., 2016). In the sub-Antarctic Kerguelen Islands, Jomelli et al. (2017) recently dated a moraine with 36Cl that is probably related to the LIA.

From a review of the available literature on LIA moraine dating in different mountain ranges, we concluded that, in general, a first glacial advance was recorded during the fourteenth century, with the major ice expansion during the seventeenth century and a last minor readvance at the beginning of the nineteenth century.

Owing to the short exposure duration of our samples, their ^{10}Be ages have 25–30% analytical uncertainties. These uncertainties are higher than the age difference of 10–16% obtained when a snow shielding correction factor is applied, as was proposed in early studies (Benson et al., 2004; Schildgen et al., 2005). In any case, this study defends the importance of considering the snow cover of the moraines studied, when applying CRE methods and when discovering the degree of degradation to which they have been subjected. The location of the glacial fronts during the LIA suggests MAAT ca. 1 °C below current values in mid-latitude mountain

regions (Oliva et al., 2018a), determining longer snow cover duration in the highlands of the glaciated massifs and strengthening shielding from cosmogenic radiation (Fig. 7). Long-lasting snow cover also intensifies nivation-related erosion processes and can intensely affect glacial deposits (Christiansen, 1998; Palacios et al., 2003).

On the other hand, as we observed in the Veleta cirque and as described in several papers cited above, the intensity of the paraglacial processes (Ballantyne, 2002; Oliva and Ruiz-Fernández, 2015) in the current deglaciation phase from the LIA advance is very high, with a complex superposition of processes that destroy the glacial landforms and accumulate new deposits on them. Therefore, as we saw, it was difficult to find suitable boulders for CRE dating in the Veleta cirque, despite its young age. In this context, the long-term study and monitoring of the dynamics of the LIA moraines in full paraglacial phase, should serve to evaluate the time needed for moraine stabilization once it has been abandoned by glacial retreat (Zreda and Phillips, 1994, Zreda and Phillips, 1995; Putkonen and O'Neal, 2006; Putkonen et al., 2008; Heyman et al., 2011) (Fig. 9).

In areas where LIA moraines are constrained by steep slopes, as is very common in Alpine systems, at least two (or possibly three) major LIA advances overlap, in some cases with other Neoglacial moraines, to form a single polygenic ridge as occurred in the Veleta cirque. This was highlighted in the mid-1980s with the concepts of obliterative overlap (Gibbons et al., 1984) and distal-flank accretion (Osborn, 1986) applied to Neoglacial advances.

5. Conclusions

The results of this research supply evidence of the very few CRE dates available on very old glacial landforms formed before the last Pleistocene glaciation and also the few very young dates available, such as those derived from LIA glaciation, compared with the large number of dates obtained for Termination I. For both periods, the selection of boulders suitable for sampling was the critical issue in Sierra Nevada, caused by intense postglacial environmental dynamics such as occurred during the last major deglaciation, which impedes the collection of a statistically significant number of samples. In the case of the LIA, moraines are still undergoing intense paraglacial readjustment to the new geomorphological setting, with very intense erosion and sediment redistribution of the unconsolidated moraine particles. In addition, moraine accretion processes during successive glacial advances are detected from

585 geomorphological observations. In moraines originating during the penultimate glaciation, the
586 long time lapse since their formation has facilitated intense erosion and reshaping of these
587 landforms, with very few stable blocks remaining on the surface since their original
588 stabilization. Periods of certain geomorphic stability may have occurred between the very old
589 and the younger glaciations (Fig. 9).

590

591 The results of this research have enabled us to verify the existence of moraines deposited in
592 glaciations prior to LPG in Sierra Nevada, as many of the first geomorphologists who studied
593 the glacial landforms of these mountains suggested, and to confirm similar CRE and OSL
594 ages established in other mountains in the northern Iberian Peninsula.

595

596 In addition, CRE dates are obtained for the first time in the Iberian Peninsula in LIA
597 moraines, with results suggesting that maximum advances during this period occurred
598 between the fourteenth and seventeenth centuries, as is the case in many other mountains
599 where the same method has been applied.

600

601 **Acknowledgments**

602 The research was carried out within the MOUNTAIN WARMING project CGL2015-65813-
603 R, Government of Spain. Marc Oliva is grateful for the support of the Ramón y Cajal research
604 program (RYC-2015-17597) and the ANTALP research group (Antarctic, Arctic, Alpine
605 Environments, 2017-SGR-1102). The ^{10}Be measurements were performed at the ASTER
606 AMS National facility (CEREGE, Aix en Provence) which is supported by the INSU/CNRS,
607 the ANR through the "Projets thématiques d'excellence" program for the "Equipements
608 d'excellence" ASTER-CEREGE action and IRD. The authors express their deep gratitude to
609 Dr. Magali Delmas and two anonymous reviewers whose detailed and interesting suggestions
610 have helped to improve our manuscript. We are also grateful to Editor Richard Marston for
611 his useful suggestions and patient editing.

612 **References**

613 Arnold, M., Merchel, S., Bourles, D., Braucher, R., Benedetti, L., Finkel, R.C., Aumaître, G.,
614 Gottdang, A., Klein, M., 2010. The French accelerator mass spectrometry facility
615 ASTER: improved performance and developments. Nucl. Instrum. Methods Phys.
616 Res. B 268, 1954-1959.

Balco, G., Stone, J. O., Lifton, N. A., Dunai, T.J., 2008. A complete and easily accessible means of calculating surface exposure ages or erosion rates from ^{10}Be and ^{26}Al measurements. Quaternary geochronology 3(3), 174-195.

Balco, G., 2011. Contributions and unrealized potential contributions of cosmogenic-nuclide exposure dating to glacier chronology, 1990–2010. Quat. Sci. Rev. 30(1-2), 3-27.

Balco, G. 2018. CRONUS-Earth online exposure age calculator v. 3. Available at: http://hess.ess.washington.edu/math/v3/v3_age_in.html (accessed _June, 2018)

Ballantyne, C.K., 2002. Paraglacial geomorphology. Quat. Sci. Rev. 21(18-19), 1935-2017.

Barrérè, P., 1953. Equilibrie glacier actuel et quaternaire dans l´Ouest des Pyrénèes Centrales. Revue geographique des Pyrénèes et du Sud-Ouest 2, 116-134.

Batbaatar, J., Gillespie, A. R., Fink, D., Matmon, A., Fujioka, T., 2018. Asynchronous glaciations in arid continental climate. Quat. Sci. Rev. 182, 1-19.

Benson, L., Madole, R., Phillips, W., Landis, G., Thomas, T., Kubik, P., 2004. The probable importance of snow and sediment shielding on cosmogenic ages of north-central Colorado Pinedale and pre-Pinedale moraines. Quat. Sci. Rev. 23, 193-206.

Bide, J.B., 1893. Deuxième excursion dans la Sierra Nevada. Annuaire du Club Alpin Français 20, 276-305.

Borchers, B., Marrero, S., Balco, G., Caffee, M., Goehring, B., Lifton, N., Nishiizumi, K., Phillips, F., Schaefer, J., Stone, J., 2016. Geological calibration of spallation production rates in the CRONUS-Earth project. Quat. Geochronol. 31, 188-198.

Braucher, R., Guillou, V., Bourles, D., Arnold, M., Aumaître, G., Keddadouche, K., Nottoli, E., 2015. Preparation of ASTER in-house ^{10}Be/^{9}Be standard solutions. Nuclear Instruments and Methods in Physics Research Section B: Beam Interactions with Materials and Atoms 361, 335-340.

Briner, J.P., Kaufman, D.S., Manley, W.F., Finkel, R.C., Caffee, M.W., 2005. Cosmogenic exposure dating of late Pleistocene moraine stabilization in Alaska. Geological Society of America Bulletin 117(7-8), 1108-1120.

Brown, E.T., Edmond, J.M., Raisbeck, G.M., Yiou, F., Kurz, M.D., Brook, E.J., 1991. Examination of surface exposure ages of Antarctic moraines using in-situ produced ^{10}Be and ^{26}Al. Geochimica Cosmochimica Acta 55, 2269-2283.

Chenet, M., Brunstein, D., Jomelli, V., Roussel, E., Rinterknecht, V., Mokadem, F., ASTER Team, 2016. ^{10}Be cosmic-ray exposure dating of moraines and rock avalanches in the Upper Romanche valley (French Alps): Evidence of two glacial advances during the Late Glacial/Holocene transition. Quat. Sci. Rev. 148, 209-221.

Chmeleff, J., von Blanckenburg, F., Kossert, K., Jakob, J., 2010. Determination of the ^{10}Be half-life by multicollector ICP-MS and liquid scintillation counting. Nucl. Instrum. Methods Phys. Res. B 268 (2), 192-199.

Clark, P.U., Dyke, A.S., Shakun, J.D., Carlson, A.E., Clark, J., Wohlfarth, B., Mitrovica, J.X., Hostetler, S.W., McCabe, A.M., 2009. The Last Glacial Maximum. Science 325, 710-714.

Christiansen, H.H., 1998. Nivation forms and processes in unconsolidated sediments, NE Greenland. Earth Surface Processes and Landforms: The Journal of the British Geomorphological Group 23(8), 751-760.

Delmas, M., 2015. The last maximum ice extent and subsequent deglaciation of the Pyrenees: an overview of recent research. Cuadernos de Investigación Geográfica 41, 359-387.

Delunel, R., Bourlès, D.L., van der Beek, P.A., Schlunegger, F., Leya, I., Masarik, J., Paquet, E., 2014. Snow shielding factors for cosmogenic nuclide dating inferred from long-term neutron detector monitoring. Quat. Geochronol. 24, 16-26. http://dx.doi.org/10.1016/j.quageo.2014.07.003.

Domínguez-Villar, D., Carrasco, R.M., Pedraza, J., Cheng, H., Edwards, R. L., Willenbring, J.K., 2013. Early maximum extent of paleoglaciers from Mediterranean mountains during the last glaciation. Scientific Reports 3, 2034.

Dong, G., Zhou, W., Yi, C., Zhang, L., Li, M., Fu, Y., Zhang, Q., 2017. Cosmogenic ^{10}Be surface exposure dating of 'Little Ice Age' glacial events in the Mount Jaggang area, central Tibet. The Holocene 27(10), 1516-1525.

Fernández-Fernández J.M., Palacios D., García-Ruiz, J.M., Andrés,N., Schimmelpfennig, I., Gómez-Villar, A., Santos-González, J., Álvarez-Martínez, J., Arnáez, J., Úbeda, J., Léanni, L., ASTER Team, 2017. Chronological and geomorphological investigation of fossil debris-covered glaciers in relation to deglaciation processes: A case study in the Sierra de La Demanda, northern Spain. Quat. Sci. Rev. 170, 232-249. doi.org/10.1016/j.quascirev.2017.06.034

García-Ruiz, J.M., Martí-Bono, C., Peña-Monné, J.L., Sancho, C., Rhodes, E.J., Valero-Garcés, B., Moreno, A., 2013. Glacial and fluvial deposits in the Aragón valley, central-western Pyrenees: chronology of the Pyrenean late pleistocene glaciers. Geografiska Annaler: Series A, Physical Geography 95(1), 15-32.

García-Ruiz, J.M., Moreno, A., González-Sampériz, P., Valero-Garcés, B., Martí-Bono, C., 2010. La cronología del último ciclo glaciar en las montañas del sur de Europa. Una revisión. Cuaternario y Geomorfología 24, 35-46.

García-Ruiz, J. M., Palacios, D., González-Sampériz, P., Andrés, N., Moreno, A., Valero-Garcés, B., Gómez-Villar, A., 2016. Mountain glacier evolution in the Iberian Peninsula during the Younger Dryas. Quat. Sci. Rev. 138, 16-30.

García-Ruiz, J.M., Palacios, D., de Andrés, N., Valero-Garcés, B.L., López-Moreno, J.I., Sanjuán, Y., 2014. Holocene and 'Little Ice Age' glacial activity in the Marboré Cirque, Monte Perdido Massif, Central Spanish Pyrenees. The Holocene 24 (11), 1439-1452. doi.org/10.1177/0959683614544053

Gibbons, A.B., Megeath, J.D., Pierce, K.L., 1984. Probability of moraine survival in a succession of glacial advances. Geology 12(6), 327-330.

Gómez-Ortiz, A., Oliva, M., Salvador-Franch, F., Salvà-Catarineu, M., Plana-Castellví, J.A., 2018. The geographical interest of historical documents to interpret the scientific evolution of the glacier existing in the Veleta cirque (Sierra Nevada, Spain) during the Little Ice Age. Cuadernos de Investigación Geográfica 44 (1), 267-292.

Gómez-Ortiz, A., Palacios, D., Oliva, M., Salvador-Franch, F., Salvà-Catarineu, M., 2015. The deglaciation of Sierra Nevada (Spain): synthesis of current knowledge and new contributions. Cuadernos de Investigación Geográfica 41 (2), 409-426.

Gómez-Ortiz, A., Palacios, D., Palade, B., Vázquez-Selem, L., Salvador-Franch, F., 2012. The deglaciation of the Sierra Nevada (southern Spain). Geomorphology 159-160, 93-105.

Gómez-Ortiz, A., Palacios, D., Palade, B., Vázquez-Selem, L., Salvador-Franch, F., Tanarro, L., Oliva, M., 2013. La evolución glaciar de Sierra Nevada y la formación de glaciares rocosos. Boletín de la Asociación de Geógrafos Españoles 61, 139-162.

Gómez-Ortiz, A., Palacios, D., Ramos, M., Tanarro, L.M., Schulte, L., Salvador, F., 2001. Location of permafrost in marginal regions: Corral del Veleta, Sierra Nevada, Spain. Permafrost and Periglacial Processes 12, 93-110.

Gómez-Ortiz, A., Palacios, D., Schulte, L., Salvador-Franch, F., Plana, J.A., 2009. Evidences from historical documents of landscape evolution after Little Ice Age of a Mediterranean high mountain area, Sierra Nevada, Spain (eighteenth to twentieth centuries). Geografiska Annaler, Series A, Physical Geography 91, 279-289.

González-Trueba, J.J., Martín, R., Martínez de Pisón, E., Serrano, E., 2008. 'Little Ice Age' glaciation and current glaciers in the Iberian Peninsula. The Holocene 18, 551-568.

716 Gosse, J.C., Phillips, F.M., 2001. Terrestrial in situ cosmogenic nuclides: theory and
717 application. Quat. Sci. Rev. 20, 1475-1560. http://dx.doi.org/10.1016/S0277-
718 3791(00)00171-2.
719 Govin, A., Capron, E., Tzedakis, P. C., Verheyden, S., Ghaleb, B., Hillaire-Marcel, C.,
720 Blunier, T., 2015. Sequence of events from the onset to the demise of the Last
721 Interglacial: Evaluating strengths and limitations of chronologies used in climatic
722 archives. Quat. Sci. Rev. 129, 1-36.
723 Graf, A., Akçar, N., Ivy-Ochs, S., Strasky, S., Kubik, P.W., Christl, M., Schlüchter, C., 2015.
724 Multiple advances of Alpine glaciers into the Jura Mountains in the Northwestern
725 Switzerland. Swiss Journal of Geosciences 108(2-3), 225-238.
726 Grant, K.M., Rohling, E.J., Bar-Matthews, M., Ayalon, A., Medina-Elizalde, M., Ramsey,
727 C.B., Roberts, A.P., 2012. Rapid coupling between ice volume and polar temperature
728 over the past 150,000 years. Nature 491(7426), 744.
729 Hallet, B., Putkonen, J., 1994. Surface Dating of dynamic landforms: Young boulders on
730 aging moraines. Science 265, 937–940.
731 Häuselmann, A.D., Fleitmann, D., Cheng, H., Tabersky, D., Günther, D., Edwards, R.L.,
732 2015. Timing and nature of the penultimate deglaciation in a high alpine stalagmite
733 from Switzerland. Quat. Sci. Rev. 126, 264-275.
734 Hempel, L., 1960. Límites altitudinales geomorfológicos en Sierra Nevada. Estudios
735 Geográficos 78, 81-93.
736 Herrero, J., Polo, M.J., 2016. Evaposublimation from the snow in the Mediterranean
737 mountains of Sierra Nevada (Spain). The Cryosphere 10(6), 2981.
738 Holzhauser, H., Magny, M., and Zumbühl, H.J., 2005. Glacier and lake-level variations in
739 west-central Europe over the last 3500 years: The Holocene 15, 789–801.
740 http://dx.doi.org/10.1191/0959683605hl853ra.
741 Hughes, P.D., 2014. Little Ice Age glaciers in the Mediterranean mountains. Mediterranée
742 122, 63-79.
743 Hughes, P.D., 2018. Little Ice Age glaciers and climate in the Mediterranean mountains: a
744 new analysis. Cuadernos de Investigación Geográfica 44 (1), 15-45.
745 Hughes, P.D., Woodward, J.C., Gibbard, P.L., 2007. Middle Pleistocene cold stage climates
746 in the Mediterranean: new evidence from the glacial record. Earth and Planetary
747 Science Letters 253(1-2), 50-56.
748 Hughes, P.D., Woodward, J.C., Van Calsteren, P.C., Thomas, L.E., 2011. The glacial history
749 of the Dinaric Alps, Montenegro. Quat. Sci. Rev. 30(23-24), 3393-3412.
750 Hughes, P.D., Woodward, J.C., Gibbard, P.L., 2006a. Glacial history of the Mediterranean
751 mountains. Progress in Physical Geography 30, 334– 364.
752 Hughes, P.D., Woodward, J.C., Gibbard, P.L., 2006b. Late Pleistocene glaciers and climate in
753 the Mediterranean region. Global and Planetary Change 46, 83–98.
754 Jiménez-Amat, P., Zahn, R., 2015. Offset timing of climate oscillations during the last two
755 glacial-interglacial transitions connected with large-scale freshwater perturbation.
756 Paleoceanography 30(6), 768-788.
757 Jomelli, V., Mokadem, F., Schimmelpfennig, I., Chapron, E., Rinterknecht, V., Favier, V.,
758 Swingedouw, D., 2017. Sub-Antarctic glacier extensions in the Kerguelen region (49°
759 S, Indian Ocean) over the past 24,000 years constrained by ^{36}Cl moraine dating. Quat.
760 Sci. Rev. 162, 128-144.
761 Jomelli, V., Lane, T., Favier, V., Masson-Delmotte, V., Swingedouw, D., Rinterknecht, V.,
762 Leanni, L., 2016. Paradoxical cold conditions during the medieval climate anomaly in
763 the Western Arctic. Scientific Reports 6, 32984.
764 Korschinek, G., Bergmaier, A., Faestermann, T., Gerstmann, U.C., Knie, K., Rugel, G.,
765 Wallner, A., Dillmann, I., Dollinger, G., von Gostomski Lierse, Ch., Kossert, K.,

766 Maitia, M., Poutivtsev, M., Remmert, A., 2010. A new value for the half-life of 10Be
767 by heavy-ion elastic recoil detection and liquid scintillation counting. Nucl. Instrum.
768 Methods Phys. Res. B 268 (2), 187-191.
769 Kotarba A., Hercman H., Dramis, F.., 2001. On the age of Campo Imperatore glaciations,
770 Gran Sasso Massif, Central Italy. Geografia Fisica e Dinamica Quaternaria 24, 65-69.
771 Le Roy, M., Deline, P., Carcaillet, J., Schimmelpfennig, I., Ermini, M., ASTER Team, 2017.
772 ^{10}Be exposure dating of the timing of Neoglacial glacier advances in the Ecrins-
773 Pelvoux massif, southern French Alps. Quat. Sci. Rev. 178, 118-138.
774 Lewis, C.J., McDonald, E.V., Sancho, C., Peña, J.L., Rhodes, E.J., 2009. Climatic
775 implications of correlated Upper Pleistocene glacial and fluvial deposits on the Cinca
776 and Gállego rivers (NE Spain) based on OSL dating and soil stratigraphy. Global and
777 Planetary Change 67, 141-152.
778 Lhenaff, R., 1977. Recherches géomorphologiques sur les Cordillères Bétiques centro-
779 occidentales (Espagne). PhD thesis, University of Lille.
780 Li, Y., Li, Y., Harbor, J., Liu, G., Yi, C., Caffee, M.W., 2016. Cosmogenic ^{10}Be constraints
781 on Little Ice Age glacial advances in the eastern Tian Shan, China. Quat. Sci. Rev.
782 138, 105-118.
783 Licciardi, J.M., Schaefer, J.M., Taggart, J.R., Lund, D.C., 2009. Holocene glacier fluctuations
784 in the Peruvian Andes indicate northern climate linkages. Science 325, 1677–1679.
785 http://dx.doi.org/10.1126/science.1175010.
786 Lifton, N., Sato, T., Dunai, T.J., 2014. Scaling in situ cosmogenic nuclide production rates
787 using analytical approximations to atmospheric cosmic-ray fluxes. Earth Planet. Sci.
788 Lett. 386, 149-160.
789 Martin, L., Blard, P.-H., Balco, G., Lave, J., Delunel, R., Lifton, N., Laurent, V., 2017. The
790 CREp program and the ICE-D production rate calibration database: a fully
791 parameterizable and updated online tool to compute cosmic-ray exposure ages. Quat.
792 Geochronol. 38, 25-49.
793 Martini, M.A., Kaplan, M.R., Strelin, J.A., Astini, R.A., Schaefer, J.M., Caffee, M.W.,
794 Schwartz, R., 2017. Late Pleistocene glacial fluctuations in Cordillera Oriental,
795 subtropical Andes. Quat. Sci. Rev. 171, 245-259.
796 Martrat, B., Jimenez-Amat, P., Zahn, R., Grimalt, J.O., 2014. Similarities and dissimilarities
797 between the last two deglaciations and interglaciations in the North Atlantic region.
798 Quat. Sci. Rev. 99, 122-134.
799 Mayewski, P.A., Rohling, E.E., Stager, C., Karlén, W., Maasch, K.A., Meeker, L.D.,
800 Meyerson, E.A., Gasse, F., Van Kreveld, S., Holmgren, K., Leethrop, J., Rosqvist, G.,
801 Rack, F., Staubwasser, M., Schneider, R.R., Steig, E.J., 2004. Holocene climate
802 variability. Quaternary Research 62 (3), 243-255.
803 Merchel, S., Herpers, U., 1999. An update on radiochemical separation techniques for the
804 determination of longlived radionuclides via Accelerator Mass Spectrometry.
805 Radiochim. Acta 84, 215-219.
806 Messerli, B., 1965. Beiträge zur Geomorphologie der Sierra Nevada (Andalusien). Juris
807 Verlag. Zürich.
808 Moseley, G.E., Spötl, C., Cheng, H., Boch, R., Min, A., Edwards, R.L., 2015. Termination-II
809 interstadial/stadial climate change recorded in two stalagmites from the north European
810 Alps. Quat. Sci. Rev. 127, 229-239.
811 Nussbaum, F., 1949. Sur les traces des glaciers quaternaires dans la région de l'Aragón.
812 Pirineos 13-14, 497-518.
813 Obermaier, H., 1914. Estudio de los glaciares de los Picos de Europa. Museo Nacional de
814 Ciencias Naturales, Madrid.

Obermaier, H., 1916. Los glaciares cuaternarios de Sierra Nevada. Trabajos del Museo Nacional de Ciencias Naturales (Geología) 17, 1-68.
Obermaier, H., Carandell, J., 1917. Los glaciares cuaternarios de la Sierra de Guadarrama. Trabajos del Museo Nacional de Ciencias Naturales, 19, 1-92.
Oliva, M., Gómez Ortiz, A. 2012. Late Holocene environmental dynamics and climate variability in a Mediterranean high mountain environment (Sierra Nevada, Spain) inferred from lake sediments and historical sources. The Holocene 22 (8), 915-927.
Oliva, M., Gómez-Ortiz, A., Palacios, D., Salvador-Franch, F., Salvà-Catarineu, M., 2014. Environmental evolution in Sierra Nevada (South Spain) since the Last Glaciation based on multi-proxy records. Quaternary International 353, 195-209.
Oliva, M., Ruiz-Fernández, J. 2015. Coupling patterns between paraglacial and permafrost degradation responses in Antarctica. Earth Surface Processes and Landforms 40 (9), 1227-1238.
Oliva, M., Ruiz-Fernández, J., Barriendos, M., Benito, G., Cuadrat, J.M., García-Ruiz, J.M., Giralt, S., Gómez-Ortiz, A., Hernández, A., López-Costas, O., López-Moreno, J.I., López-Sáez, J.A., Martínez-Cortizas, A., Moreno, A., Prohom, M., Saz, M.A., Serrano, E., Tejedor, E., Trigo, R., Valero-Garcés, B., Vicente-Serrano, S., 2018a. The Little Ice Age in Iberian mountains. Earth Science Reviews 177, 175-208.
Oliva, M., Žebre, M., Guglielmin, M., Çiner, A., Vieira, G., Bodin, X., Andrés, N., Colucci, R.R., García-Hernández, C., Hughes, P., Mora, C., Nofre, J., Palacios, D., Pérez-Alberti, A., Ribolini, A., Ruiz-Fernández, J., Sarıkaya, M.A., Serrano, E., Urdea, P., Valcárcel, M., Woodward, J., Yıldırım, C., 2018b. Permafrost conditions in the Mediterranean region since the Last Glaciation. Earth-Science Reviews 185, 397-436.
Oliva, M., Serrano, E., Gómez-Ortiz, A., González Amuchastegui, M.J., Nieuwendam, A., Palacios, D., Pellitero-Ondicol, R., Pérez-Alberti, A., Ruiz-Fernández, J., Valcárcel, M., Vieira, G., 2016b. Spatial and temporal variability of periglaciation of the Iberian Peninsula. Quat. Sci. Rev., 137, 176-199.
Oliva, M., Gómez Ortiz, A., Salvador-Franch, F., Salvà-Catarineu, M., Ramos, M., Palacios, D., Tanarro, L., Pereira, P., Ruiz-Fernández, J., 2016a. Inexistence of permafrost at the top of Veleta peak (Sierra Nevada, Spain). Science of the Total Environment 550, 484-494.
Oppo, D.W., J.F. McManus, Cullen, J. L., 2006. Evolution and demise of the last interglacial warmth in the subpolar North Atlantic, Quat. Sci. Rev. 25, 3268–3277.
Osborn, G., 1986. Lateral-moraine stratigraphy and neoglacial history of Bugaboo Glacier, British Columbia. Quaternary Research 26(2), 171-178.
Palacios, D., de Andrés, N., Luengo, E., 2003. Distribution and effectiveness of nivation in Mediterranean mountains: Peñalara (Spain). Geomorphology 54(3-4), 157-178.
Palacios, D., Andrés, N., Gòmez-Ortiz, A., García-Ruiz, J.M., 2017a. Evidence of glacial activity during the Oldest Dryas in the Mountain of Spain. In: Hughes, P. and Woodward, J. (Eds.) Quaternary glaciation in the Mediterranean Mountains. Geological Society of London, Special Publication, 433(1), 87-110. doi.org/10.1144/SP433.10
Palacios, D., García-Ruiz, J.M., Andrés, N., Schimmelpfennig, I., Campos, N. Leanni, L., ASTER Team, 2017b. Deglaciation in the central Pyrenees during the Pleistocene-Holocene transition: Timing and geomorphological significance. Quat. Sci. Rev. 162, 111-127. doi.org/10.1016/j.quascirev. 2017.03.007
Palacios, D., Gómez Ortiz, Andres, N., Salvador, F., Oliva, M., 2016. A Timing and new geomorphologic evidence of the last deglaciation stages in Sierra Nevada (southern Spain) Quat. Sci. Rev. 150, 110-129 doi.org/10.1016/j.quascirev.2016.08.012
Palma, P., Oliva, M., García-Hernández, C., Gómez Ortiz, A., Ruiz-Fernández, J., Salvador-Franch, F., Catarineu, M., 2017. Spatial characterization of glacial and periglacial

landforms in the highlands of Sierra Nevada (Spain). Sci. Total Environ. 584–585, 1256–1267. https://doi.org/10.1016/j.scitotenv.2017.01.196

Penck, A., 1883. La période glaciaire dans les Pyrénées. Bulletin de la Société d'Histoire Naturelle de Toulouse 19, 105-200.

Penck, A., 1897. Die Picos de Europa und das kantabrische Gebirge. Geographische Zeitschrift, 278-281.

Putkonen, J., Connolly, J., Orloff, T., 2008. Landscape evolution degrades the geologic signature of past glaciations. Geomorphology 97, 208-217.

Putkonen, J., O'Neal, M., 2006. Degradation of unconsolidated Quaternary landforms in the western North America. Geomorphology 75, 408-419.

Quelle, O., 1908. Beiträge zur Kenntnis der spanischen Sierra Nevada. Friedrich-Wilheilms Universität, Berlin.

Rodríguez-Rodríguez, L., Jiménez-Sánchez, M., Domínguez-Cuesta, M.J., Rinterknecht, V., Pallàs, R., Bourlès, D., 2016. Chronology of glaciations in the Cantabrian Mountains (NW Iberia) during the Last Glacial Cycle based on in situ-produced ^{10}Be. Quat. Sci. Rev. 138, 31-48.

Rodríguez-Rodríguez, L., Jiménez-Sánchez, M., Domínguez-Cuesta, M.J., Rinterknecht, V., Pallàs, R., Aumaître, G., Bourlès, D.L., Keddadouche, K., 2017. Timing of last deglaciation in the Cantabrian Mountains (Iberian Peninsula; North Atlantic Region) based on in situ-produced ^{10}Be exposure dating. Quat. Sci. Rev. 171, 166–181. https://doi.org/10.1016/j.quascirev.2017.07.012

Rohling, E.J., Hibbert, F.D., Williams, F.H., Grant, K.M., Marino, G., Foster, G. L., Webster, J.M., 2017. Differences between the last two glacial maxima and implications for ice-sheet, δ^{18}O, and sea-level reconstructions. Quat. Sci. Rev. 176, 1-28.

Sánchez-Gómez, S., 1990. Aplicación del estudio de suelos a la dinámica de la cuenca del río Lanjarón. Relación suelos-geomorfología. PhD thesis, University of Granada.

Sanz de Galdeano, C., López-Garrido, A.C., 1999. Nature and impact of the Neotectonic deformation in the western Sierra Nevada (Spain). Geomorphology 30 (3), 259-272.

Schaefer, J.M., Oberholzer, P., Zhao, Z., Ivy-Ochs, S., Wieler, R., Baur, H., Schlüchter, C. 2008. Cosmogenic beryllium-10 and neon-21 dating of late Pleistocene glaciations in Nyalam, monsoonal Himalayas. Quat. Sci. Rev. 27(3-4), 295-311.

Schaefer, J.M., Denton, G.H., Kaplan, M., Putnam, A., Finkel, R.C., Barrell, D.J.A., Andersen, B.G., Schwartz, R., Mackintosh, A., Chinn, T., Schlüchter, C., 2009. High frequency Holocene glacier fluctuations in New Zealand differ from the northern signature. Science 324, 622–625. http://dx.doi.org/10.1126/science.1169312.

Schildgen, T.F., Phillips, W.M., Purves, R.S., 2005. Simulation of snow shielding corrections for cosmogenic nuclide surface exposure studies. Geomorphology 64, 67–85.

Schimmelpfennig, I., Schaefer, J.M., Akçar, N., Ivy-Ochs, S., Finkel, R.C., Schlüchter, C., 2012. Holocene glacier culminations in the Western Alps and their hemispheric relevance. Geology 40, 891–894. doi:10.1130/G33169.1

Schimmelpfennig, I., Schaefer, J.M., Akçar, N., Koffman, T., Ivy-Ochs, S., Schwartz, R., Finkel, R.C., Zimmerman, S., Schlüchter, C., 2014. A chronology of Holocene and Little Ice Age glacier culminations of the Steingletscher, Central Alps, Switzerland, based on high-sensitivity beryllium-10 moraine dating. Earth and Planetary Science Letters 393, 220-230.

Styllas, M.N., Schimmelpfennig, I., Benedetti, L., Ghilardi, M., ASTER Team, 2018. Late-glacial and Holocene history of the northeast Mediterranean mountains-New insights from in situ-produced 36Cl-based cosmic ray exposure dating of paleo-glacier deposits on Mount Olympus, Greece. Quat. Sci. Rev. 193, 244-265.

914 Uppala, S.M., Kållberg, P., Simmons, A., Andrae, U., Bechtold, V., Fiorino, M., Gibson, J.,
915 Woollen, J., 2005. The ERA-40 reanalysis. Q.J.R. Meteorological Soc. 131, 2961-
916 3012.
917 Vidal-Romaní, J.R., Fernández-Mosquera, D., Marti, K., 2015. The glaciation of Serra de
918 Queixa-Invernadoiro and Serra do Gerês-Xurés, NW Iberia. A critical review and a
919 cosmogenic nuclide (^{10}Be and ^{21}Ne) chronology. Cadernos do Laboratorio Xeolóxico
920 de Laxe 38, 25-44.
921 Villa, E., Stoll, H., Farias, P., Adrados, L., Edwards, R.L., Cheng, H., 2013. Age and
922 significance of the Quaternary cemented deposits of the Duje Valley (Picos de
923 Europa, Northern Spain). Quaternary Research 79, 1-5.
924 Young, N.E., Schweinsberg, A.D., Briner, J.P., Schaefer, J.M., 2015. Glacier maxima in
925 Baffin Bay during the Medieval Warm Period coeval with Norse settlement. Science
926 advances 1(11), e1500806.
927 Zreda, M.G., Phillips, F.M., 1995. Insights into alpine moraine development from cosmogenic
928 ^{36}Cl buildup dating. Geomorphology 14(2), 149-156.
929 Zreda, M.G., Phillips, F.M., 1994. Cosmogenic ^{36}Cl accumulation in unstable landforms.
930 Water Resources Research 30, 3127–3136.
931 Zweck, C., Zreda, M., Desilets, D., 2013. Snow shielding factors for cosmogenic nuclide
932 dating inferred from Monte Carlo neutron transport simulations. Earth Planet Sci.
933 Lett. 379, 64-71. http://dx.doi.org/10.1016/j.epsl.2013.07.023.
934

935
936 Table 1. Current knowledge of Quaternary glacial stages in Sierra Nevada.

Stage	Chronology	Processes and landforms
Pre-Last Glaciation	unknown	Possible existence of eroded moraines from glaciations occurred before the Last Glaciation as well as glacio-fluvial sediments distributed at lower elevations than moraines formed during the Last Glaciation (Hempel, 1960; Messerli, 1965; Lhenaff, 1977; Sánchez-Gómez, 1990).
Last Glaciation (Maximum Ice Extent; MIE)	Two glacial advances at ca. 30-32 ka and 19-20 ka	Development of alpine valleys at elevations between 2000 and 2500 m in northern and southern slopes, respectively (Gómez-Ortiz et al., 2012, Gómez-Ortiz et al., 2013, Gómez-Ortiz et al., 2015; Oliva et al., 2014; Palacios et al., 2016). The glaciated environment during the MIE encompassed105 km^2 (Palma et al., 2017).
Deglaciation	Two glacial advances during the Oldest Dryas (OD) at ca. 17 ka and Younger Dryas (YD) at ca. 12-13 ka	Glacial retreat at ca. 19 ka followed by two phases of glacial development until the Holocene, mainly in the highest valleys from the northern slope of the massif (Gómez-Ortiz et al., 2012, Gómez-Ortiz et al., 2013; Oliva and Gómez-Ortiz, 2012; Oliva et al., 2014; Palacios et al., 2016).
Holocene	Glacial retreat until the Early Holocene at ca. 9-10 ka	The glaciers formed during the YD finally melted and paraglacial activity favoured the development of rock glaciers in these areas (Gómez-Ortiz et al., 2012, Gómez-Ortiz et al., 2013; Oliva et al., 2016b; Palacios et al., 2016).
	Three stages with formation of glaciers occurred during the Late Holocene at ca. 2.8-2.7, 1.4-1.2 ka cal BP and LIA	Lake sediments suggest the development of a small glacier in the Mulhacén cirque, which is reflected in several moraine ridges distributed across the cirque floor (Oliva and Gómez-Ortiz, 2012; Oliva et al., 2015).
LIA	From 1440 to 1710 CE a glacier existed in the Mulhacén cirque, and another glacier developed in the Corral de Veleta cirque until the mid-20th century.	In the highest northern cirques between Mulhacén and Veleta peaks, historical sources and geomorphic evidence (i.e. moraines) shows evidence of the existence of several small glaciers that gradually disappeared during the 19th and 20th centuries (Gómez-Ortiz et al., 2001, Gómez-Ortiz et al., 2009, Gómez-Ortiz et al., 2018; Oliva and Gómez-Ortiz, 2012; Oliva et al., 2018a).

937

Table 2. Field data and characteristics of boulder samples dated with ^{10}Be in Sierra Nevada (*boulders are covered by snow thickness of 30 to 130 cm during 8 months per year). See text for details.

Sample	Latitude (ºN)	Longitude (ºW)	Elevation (m a.s.l.)	Thickness (cm)	Topographic Shielding factor	Snow Shielding factor
NAUT-1	37.0196111	3.33047222	2164	1.5	0.97832	
NAUT-2	37.0201111	3.33036111	2179	1.5	0.98414	
NAUT-3	37.02125	3.32977778	2211	1.5	0.98221	
NAUT-4	37.0225556	3.32866667	2263	3.0	0.97817	
SN-11-1	37.0595833	3.36569444	3076	2.5	0.80979	0.70067
SN-11-2	37.0605833	3.36747222	3061	2.0	0.80979	0.70067
SN-11-3	37.0606944	3.36897222	3095	2.0	0.80979	0.70067

Table 3. Analytical data and ^{10}Be sample exposure ages.

Sample	Quartz (g)	^{9}Be carrier solution (mg) [a]	^{10}Be/^{9}Be (x10^{13}) [b]	[10Be] (x10^{3} at.g^{-1})	10Be age (CREp [c]) (ka)	10Be age (C-E [d]) (ka)	10Be age (CREp [c]) (ka) With snow shielding factor	10Be age (C-E [d]) (ka) With snow shielding factor
NAUT-1	18.32	98.9	23.3 ± 1.0	2530 ± 110	134.8 ± 10 (6.2)	130.4 ± 10 (6.1)		
NAUT-2	21.98	100.2	11.2 ± 0.58	1030 ± 53	53.7 ± 4.3 (2.9)	54.5 ± 4.3 (2.9)		
NAUT-3	22.53	100.5	9.62 ± 0.55	868 ± 50	43.8 ± 3.2 (2.3)	43.0 ± 3.6 (2.5)		
NAUT-4	22.62	100.7	28.6 ± 1.2	2580 ± 110	129.2 ± 8.9 (5.4)	125.4 ± 9.4 (5.5)		
SN-11-1	30.91	100.9	0.127 ±0.052	8.4 ± 3.5	0.31 ± 0.10 (0.10)	0.28 ± 0.11 (0.11)	0.34 ± 0.12 (0.12)	0.32 ± 0.13 (0.13)
SN-11-2	32.79	100.7	0.285 ± 0.086	17.7 ± 5.3	0.60 ± 0.22 (0.21)	0.59 ± 0.20 (0.18)	0.72 ± 0.28 (0.27)	0.71 ± 0.22 (0.22)
SN-11-3	31.39	101.0	0.159 ± 0.050	10.3 ± 3.3	0.36 ± 0.09 (0.09)	0.35 ± 0.11 (0.10)	0.40 ± 0.11 (0.11)	0.38 ± 0.12 (0.12)
Blank		99.4	0.0450 ± 0.013					

[a] Carrier has a concentration of 3025 µg ^{9}Be/g.
[b] Sample ^{10}Be/^{9}Be ratios corrected for batch-specific analytical blank ratio of (4.5 ± 1.3) x 10^{-15}.
[c] ^{10}Be ages calculated with the online CREp exposure age calculator (Martin et al., 2017). 1sigma errors include analytical and production rate uncertainties; analytical errors shown in brackets.
[d] ^{10}Be ages calculated with the online exposure age calculator formerly known as the CRONUS-Earth online exposure age calculator version 3 (Balco et al., 2008). 1sigma errors include analytical and production rate uncertainties; analytical errors shown in brackets.

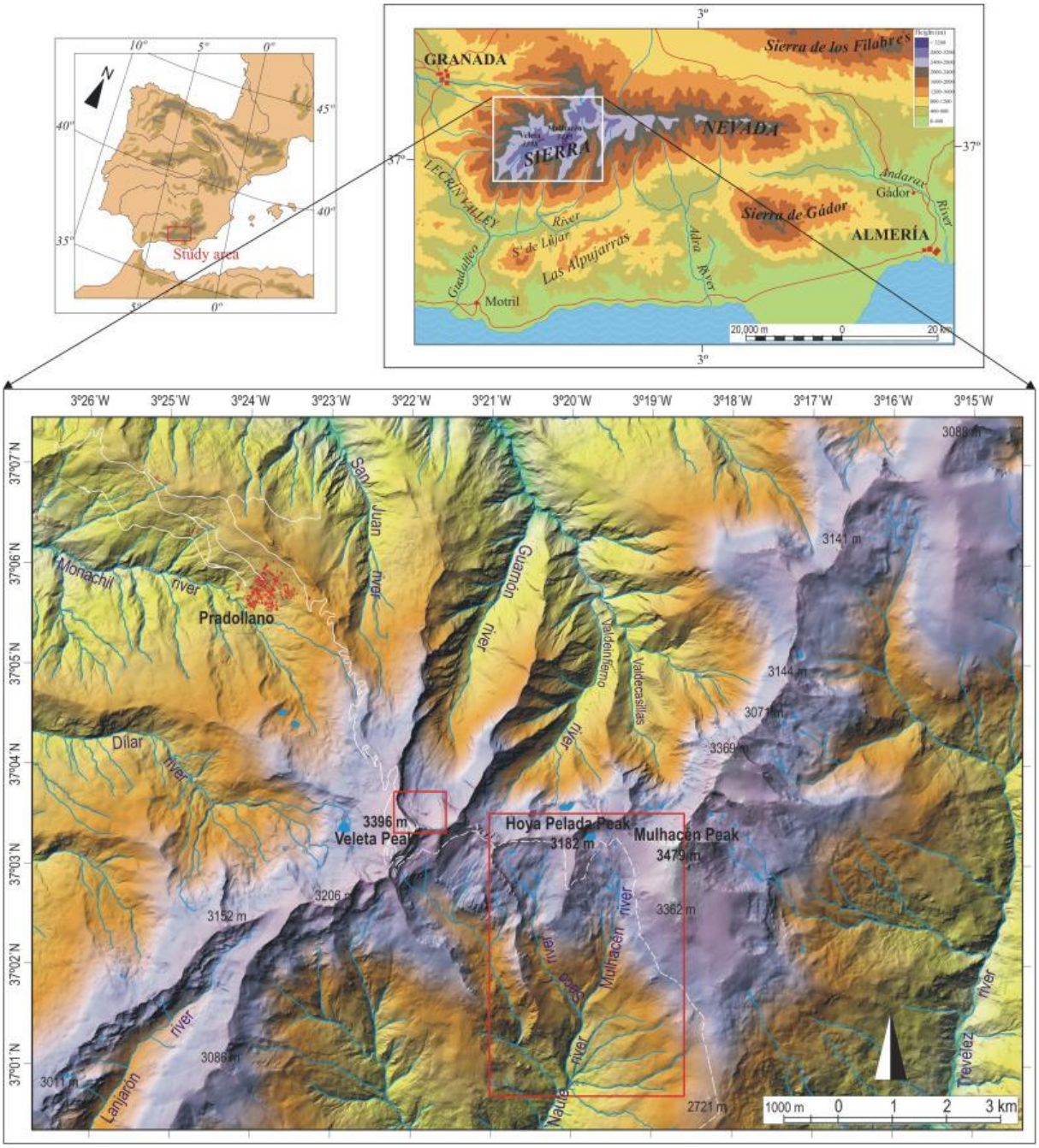
Study area
GRANADA
Sierra de los Filabres
NEVADA
SIERRA
LECRÍN VALLEY
Sierra de Gádor
ALMERÍA
Las Alpujarras
Motril
Gádor
Andarax River
Adra River
Guadalfeo River
S.ª de Lújar
20,000 m 0 20 km
3°26'W 3°25'W 3°24'W 3°23'W 3°22'W 3°21'W 3°20'W 3°19'W 3°18'W 3°17'W 3°16'W 3°15'W
37°07'N 37°06'N 37°05'N 37°04'N 37°03'N 37°02'N 37°01'N
Monachil river
Pradollano
Dílar river
Lanjarón river
Sant Juan river
Guarnón river
Valdeinfierno river
Valdecasillas river
Poqueira river
Mulhacén river
Trevélez river
Veleta Peak
3396 m
Hoya Pelada Peak
3182 m
Mulhacén Peak
3479 m
3088 m
3141 m
3144 m
3071 m
3369 m
3206 m
3152 m
3362 m
3086 m
3011 m
2721 m
1000 m 0 1 2 3 km

954

955

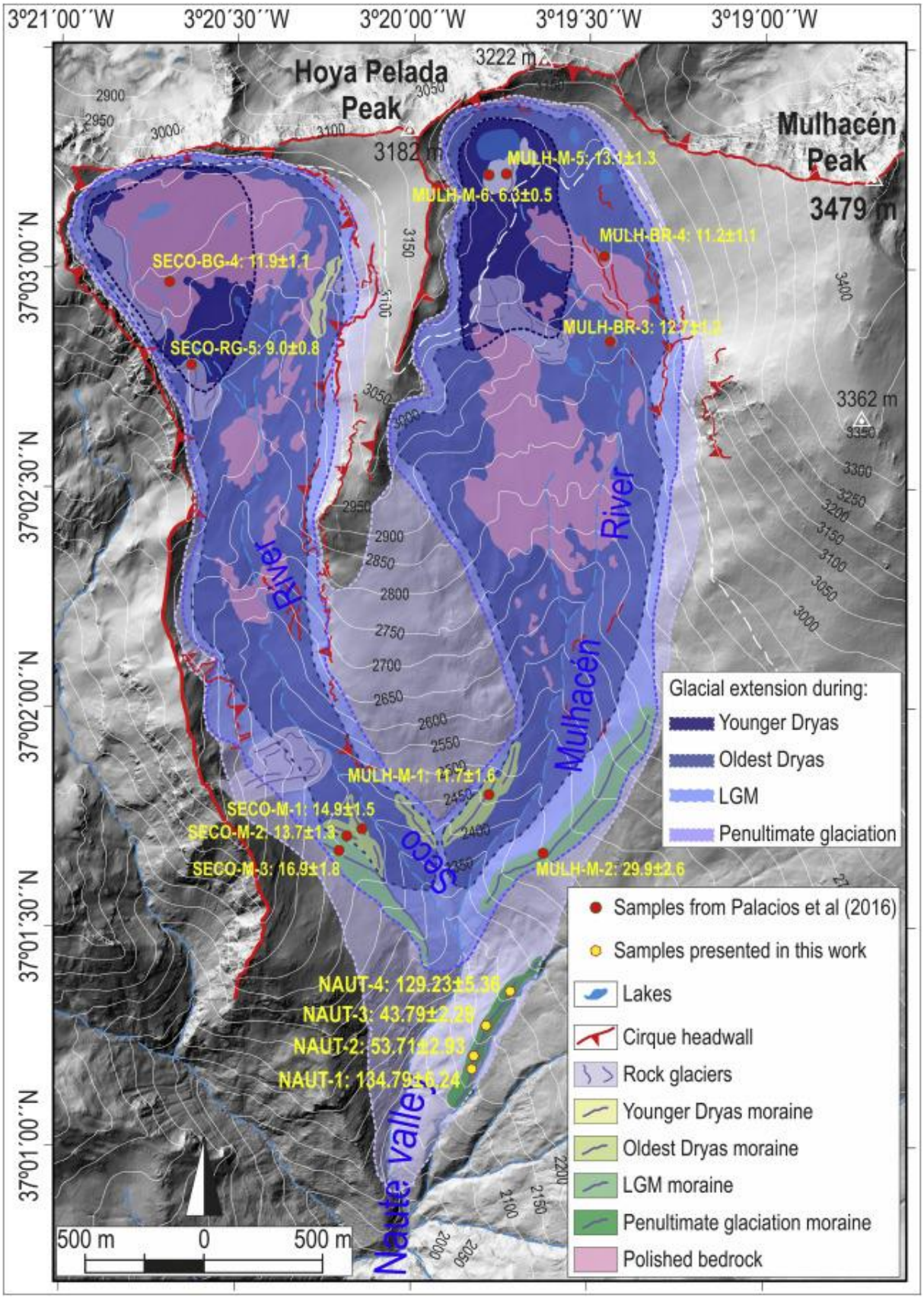
3º21´00´´W
3º20´30´´W
3º20´00´´W
3º19´30´´W
3º19´00´´W
37º03´00´´N
37º02´30´´N
37º02´00´´N
37º01´30´´N
37º01´00´´N
Hoya Pelada Peak
3182 m
3222 m
Mulhacén Peak
3479 m
3362 m
MULH-M-5: 13.1±1.3
MULH-M-6: 6.3±0.5
MULH-BR-4: 11.2±1.1
MULH-BR-3: 12.7±1.2
SECO-BG-4: 11.9±1.1
SECO-RG-5: 9.0±0.8
MULH-M-1: 11.7±1.6
SECO-M-1: 14.9±1.5
SECO-M-2: 13.7±1.3
SECO-M-3: 16.9±1.8
MULH-M-2: 29.9±2.6
NAUT-4: 129.23±5.36
NAUT-3: 43.79±2.20
NAUT-2: 53.71±2.93
NAUT-1: 134.79±6.24
Seco River
Mulhacén River
Naute valley
Glacial extension during:
Younger Dryas
Oldest Dryas
LGM
Penultimate glaciation
Samples from Palacios et al (2016)
Samples presented in this work
Lakes
Cirque headwall
Rock glaciers
Younger Dryas moraine
Oldest Dryas moraine
LGM moraine
Penultimate glaciation moraine
Polished bedrock
500 m
0
500 m

956

957

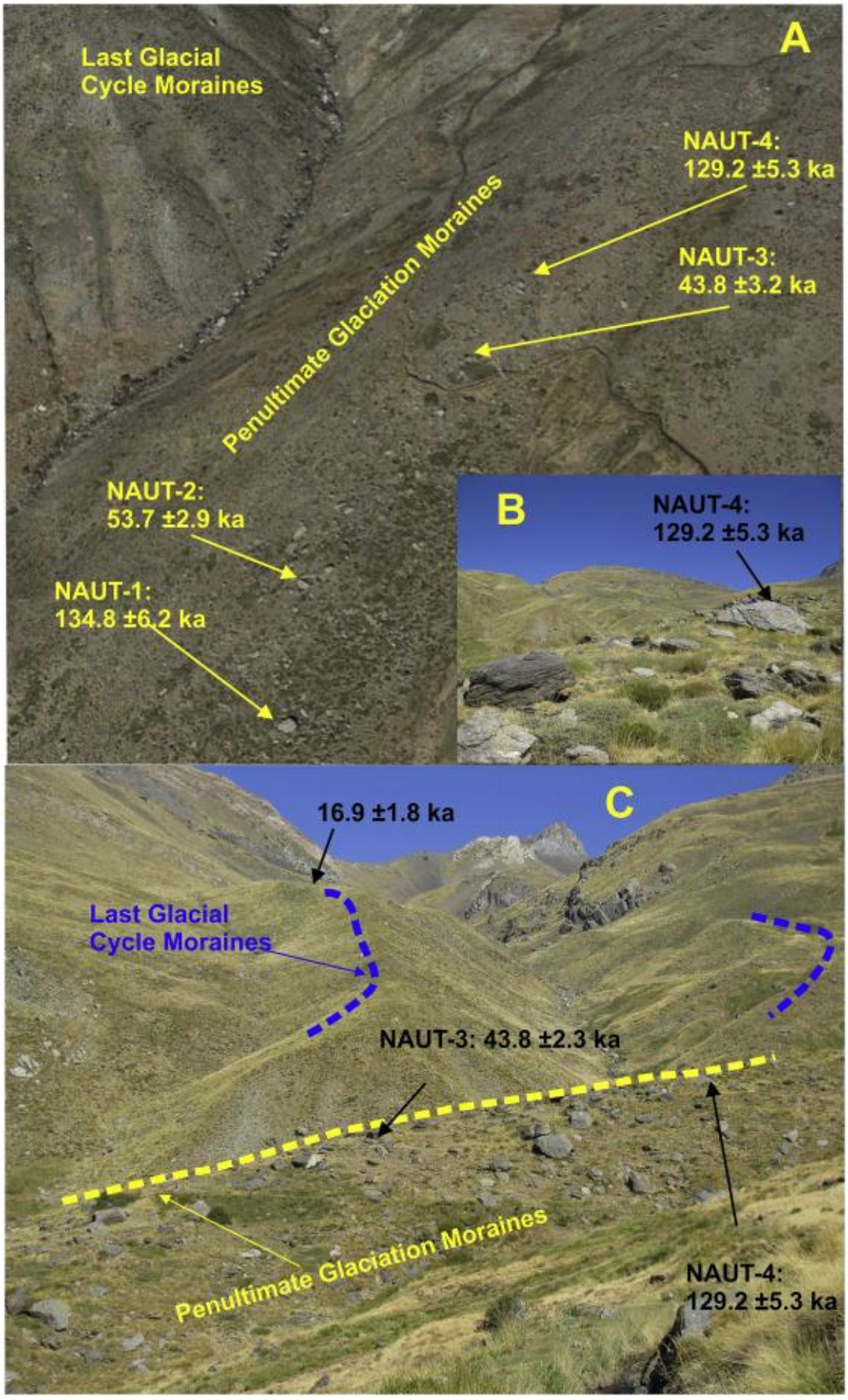
A
Last Glacial
Cycle Moraines
NAUT-4:
129.2 ±5.3 ka
NAUT-3:
43.8 ±3.2 ka
Penultimate Glaciation Moraines
NAUT-2:
53.7 ±2.9 ka
NAUT-1:
134.8 ±6.2 ka
B
NAUT-4:
129.2 ±5.3 ka
C
16.9 ±1.8 ka
Last Glacial
Cycle Moraines
NAUT-3: 43.8 ±2.3 ka
Penultimate Glaciation Moraines
NAUT-4:
129.2 ±5.3 ka

958

959

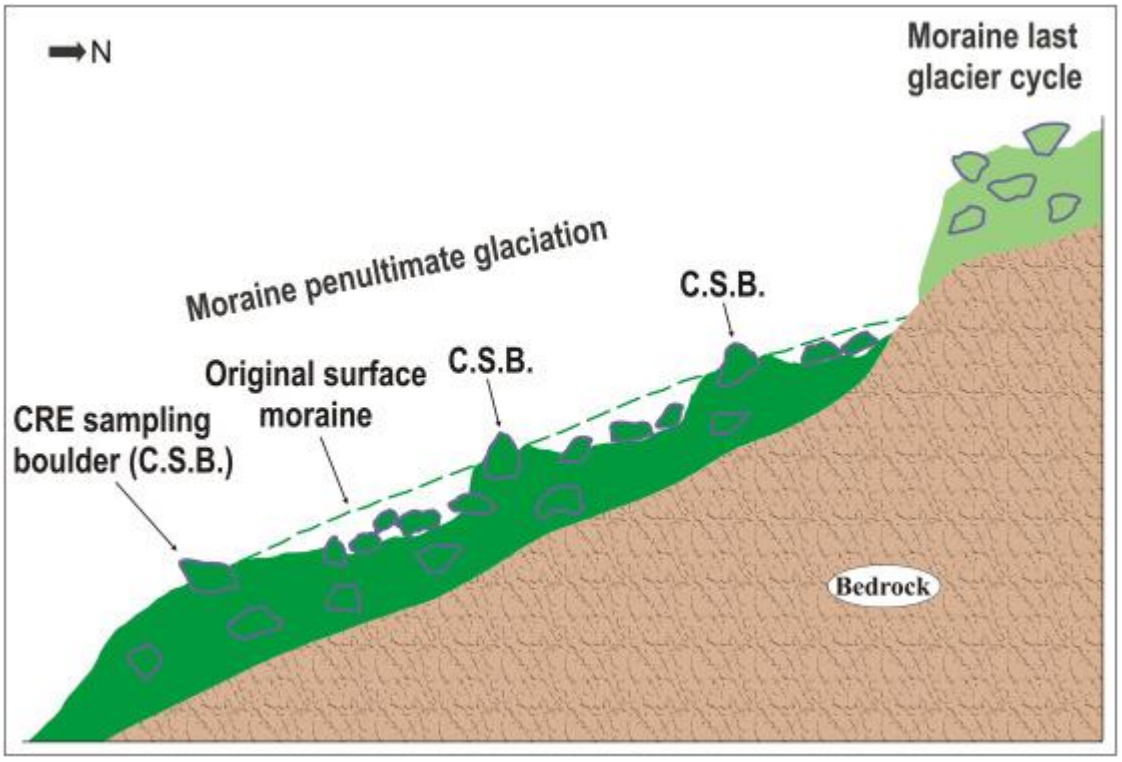
N
Moraine last glacier cycle
Moraine penultimate glaciation
C.S.B.
C.S.B.
Original surface moraine
CRE sampling boulder (C.S.B.)
Bedrock

960

961

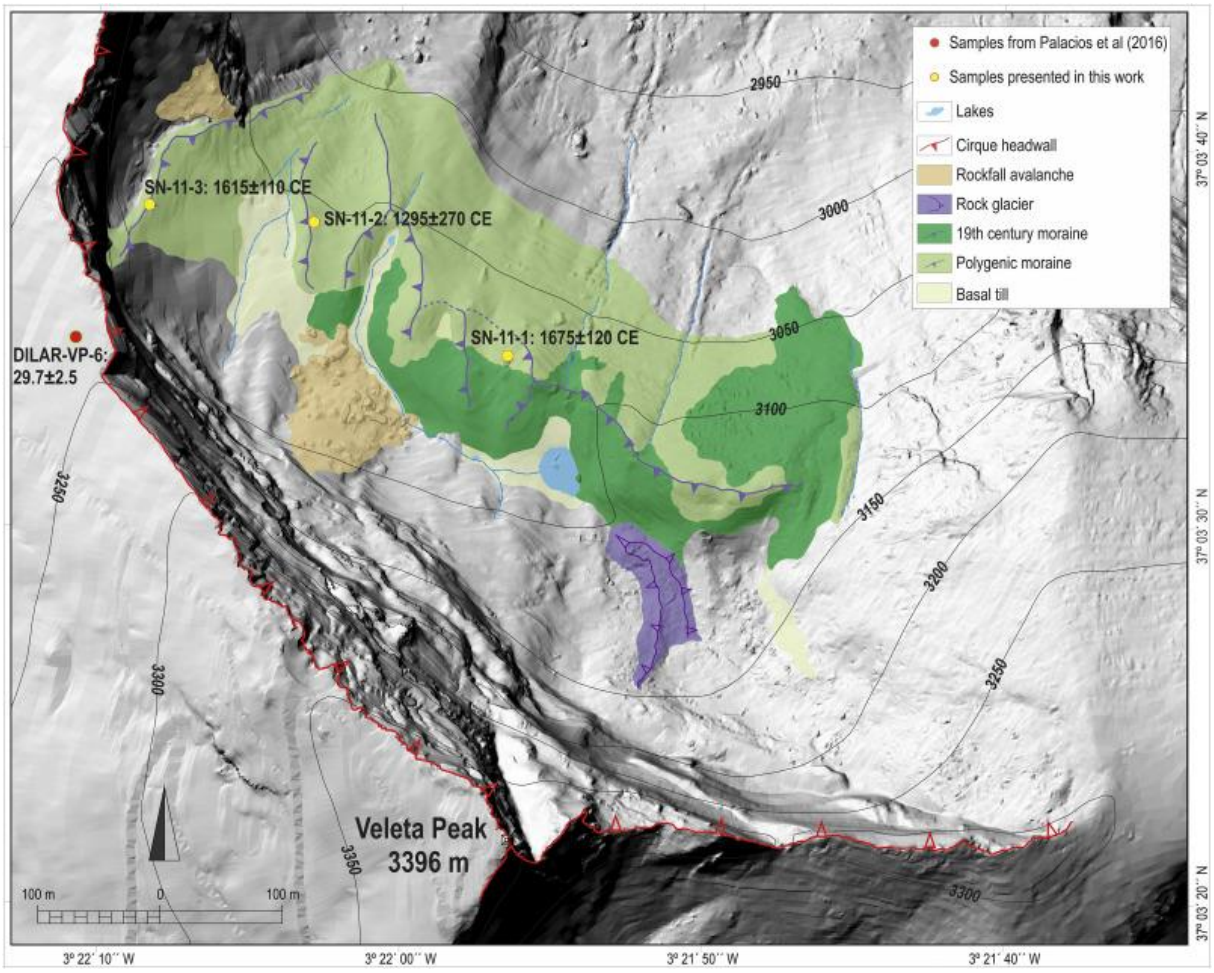
Samples from Palacios et al (2016)
Samples presented in this work
Lakes
Cirque headwall
Rockfall avalanche
Rock glacier
19th century moraine
Polygenic moraine
Basal till
SN-11-3: 1615±110 CE
SN-11-2: 1295±270 CE
SN-11-1: 1675±120 CE
DILAR-VP-6:
29.7±2.5
Veleta Peak
3396 m
2950
3000
3050
3100
3150
3200
3250
3300
3350
100 m
0
100 m
3° 22' 10'' W
3° 22' 00'' W
3° 21' 50'' W
3° 21' 40'' W
37° 03' 40'' N
37° 03' 30'' N
37° 03' 20'' N

962

963

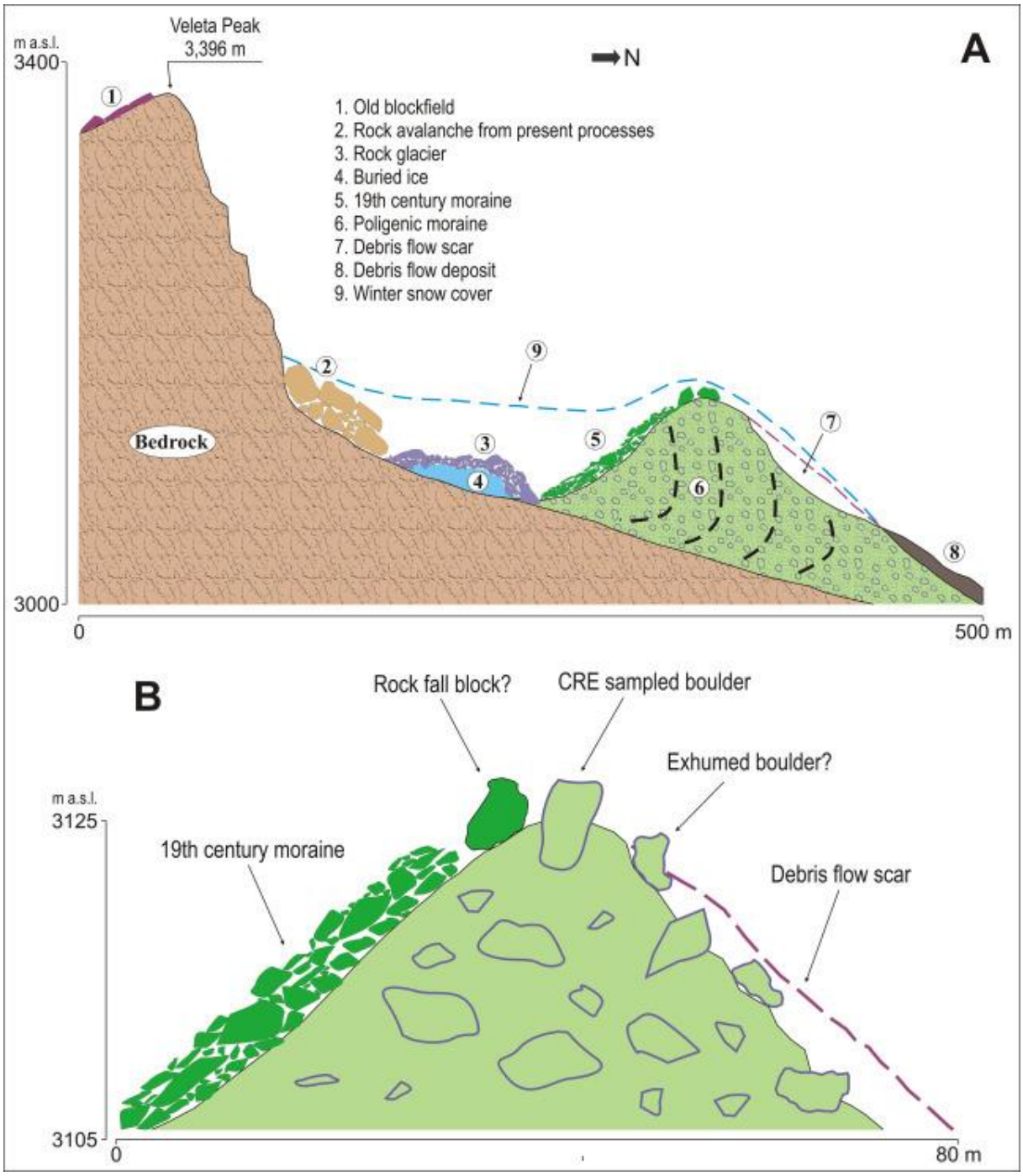
A
m a.s.l.
3400
3000
Veleta Peak
3,396 m
N
1. Old blockfield
2. Rock avalanche from present processes
3. Rock glacier
4. Buried ice
5. 19th century moraine
6. Poligenic moraine
7. Debris flow scar
8. Debris flow deposit
9. Winter snow cover
Bedrock
0
500 m
B
Rock fall block?
CRE sampled boulder
Exhumed boulder?
m a.s.l.
3125
3105
19th century moraine
Debris flow scar
0
80 m

964

965

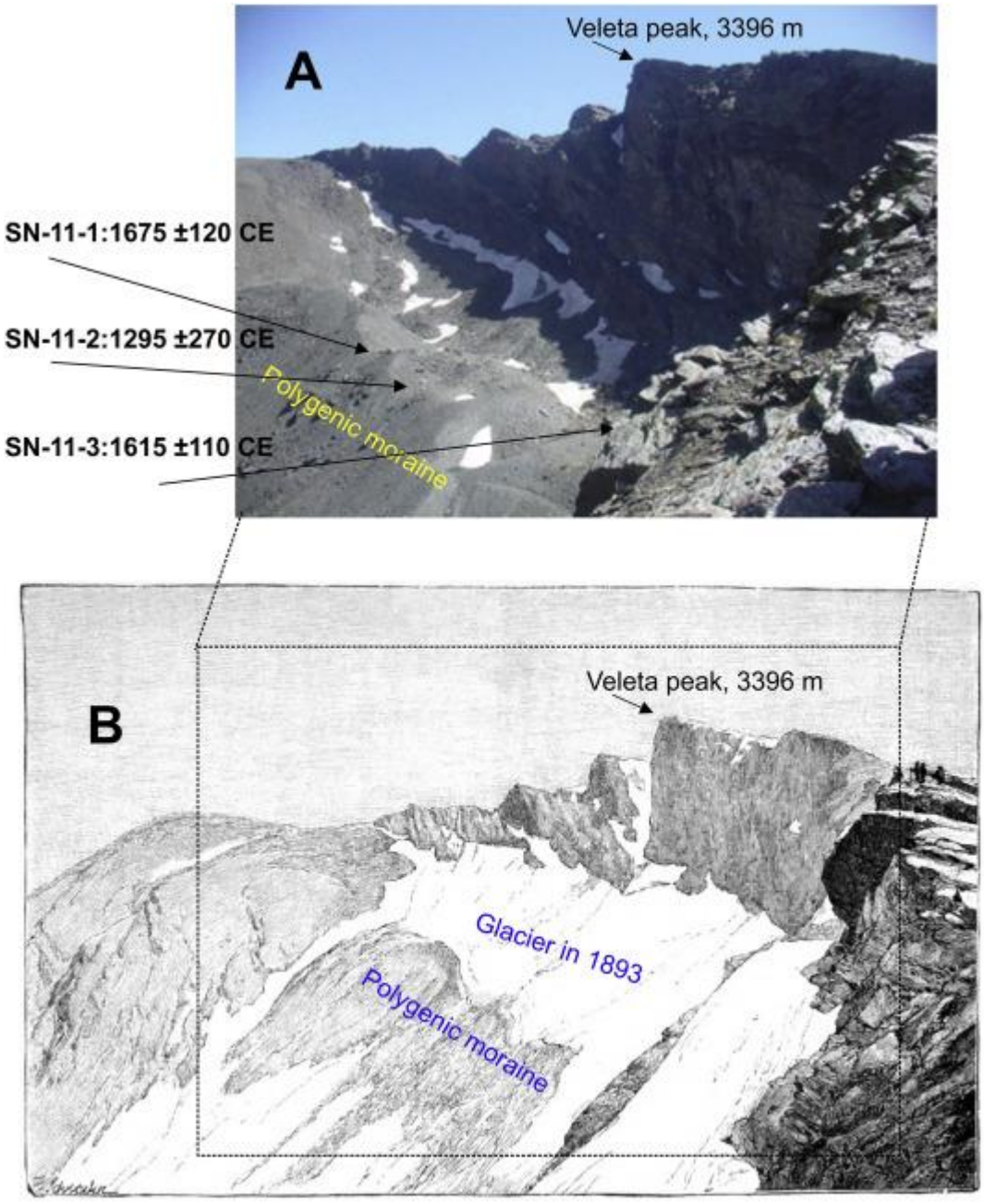
A
Veleta peak, 3396 m
SN-11-1:1675 ±120 CE
SN-11-2:1295 ±270 CE
SN-11-3:1615 ±110 CE
Polygenic moraine
B
Veleta peak, 3396 m
Glacier in 1893
Polygenic moraine

966

967

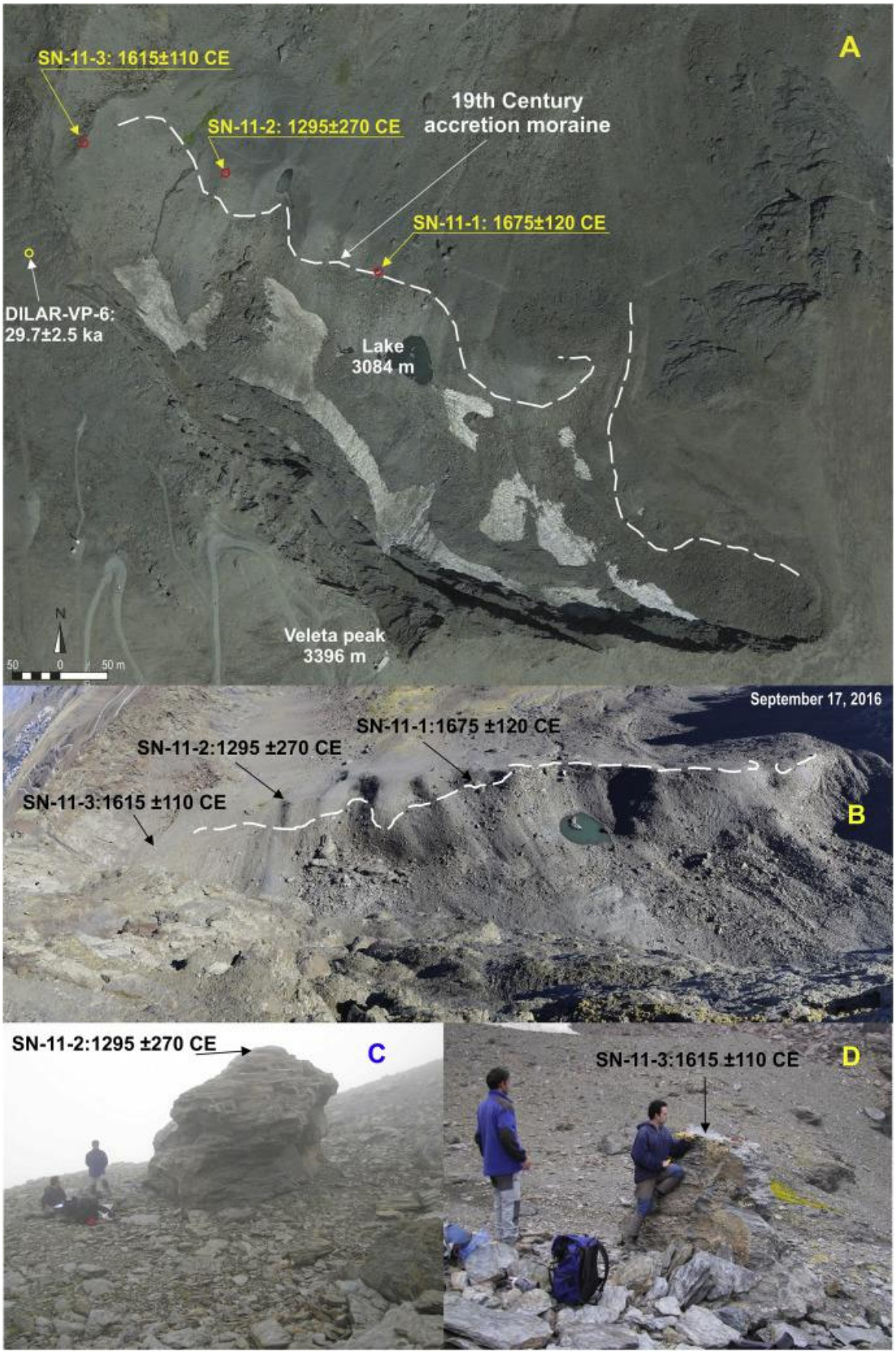
A
SN-11-3: 1615±110 CE
SN-11-2: 1295±270 CE
19th Century
accretion moraine
SN-11-1: 1675±120 CE
DILAR-VP-6:
29.7±2.5 ka
Lake
3084 m
Veleta peak
3396 m
N
50 0 50 m
September 17, 2016
SN-11-1:1675 ±120 CE
SN-11-2:1295 ±270 CE
SN-11-3:1615 ±110 CE
B
SN-11-2:1295 ±270 CE
C
SN-11-3:1615 ±110 CE
D

968

969

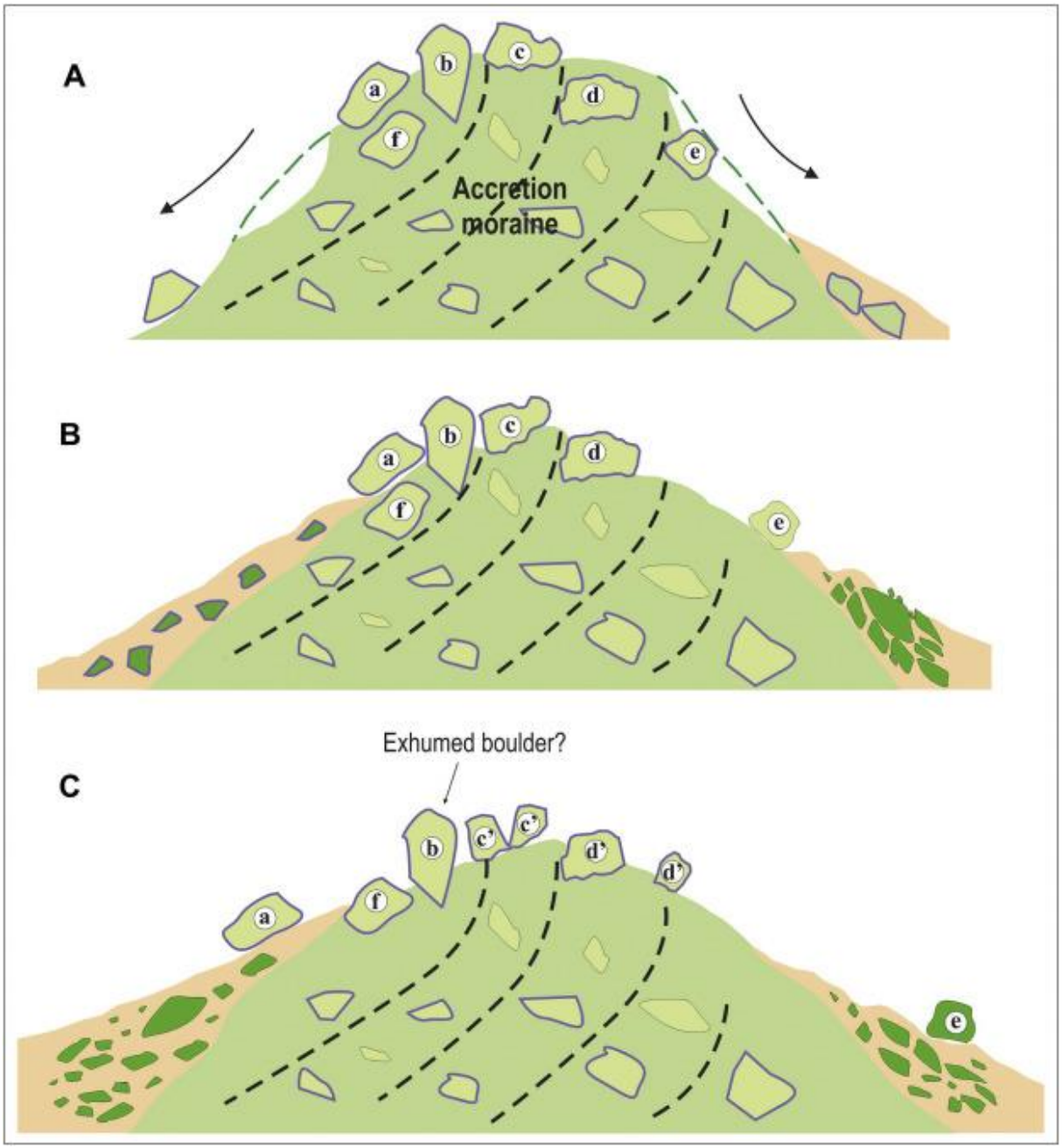
A
a
b
c
d
e
f
Accretion
moraine
B
a
b
c
d
e
f
C
Exhumed boulder?
a
b
c'
c'
d'
d'
e
f

970

971

Figure captions

Figure 1. Location of the case of study area, Sierra Nevada, in the south of the Iberian Peninsula.

Figure 2. Geomorphological map of the Naute valley and location of samples. We show CRE ages from this work (NAUT samples) together with those from Palacios et al. (2016).

Figure 3. Results of the Naute moraine samples of this work, together with pictures of some of the sampled boulders and CRE data (including data from Palacios et al. (2016)). (A) Penultimate glaciation moraine (source: Google Earth imagery), (B) Picture of the sampled NAUT-4 boulder, (C) Panoramic view of the penultimate glaciation moraine next to the last glacial cycle moraine.

Figure 4. Geomorphological sketch of the two moraines existing in the lower part of the Naute valley, together with the location of the CRE Sampling Boulder (CSB).

Figure 5. Geomorphological map of the Veleta cirque and sample location. We show CRE ages from this work (NAUT samples) together with those from Palacios et al. (2016).

Figure 6. (A) Schematic transect of the Veleta cirque including the different landforms existing across the cirque floor, and (B) Sketch showing the geomorphological approach used in the selection of samples in the Veleta cirque.

Figure 7. (A) Photo of Corral of the Veleta cirque from the West in September, 2016. (B) Drawing according to the vision of Bide (1893), where the glacier seems still to cover its maximum extension in 19th century.

Figure 8. (A) Veleta cirque with its 19th century moraine (source: Google Earth), (B) Vertical view of the Veleta cirque floor from the Veleta peak, (C) Sampled boulder for SN-11-2, and (D) Sampled boulder for SN-11-3.

Figure 9. Sketch representing the erosion processes affecting a moraine: (A) Intense mass movements and erosion reshaping the main ridge during the paraglacial stage, (B) Stabilization phase of a moraine at the end of paraglacial phase, and (C) Mature stage of an old moraine after a long period of erosion.